ADVANCED RESEARCH PROJECTS AGENCY
Contract SD-88

Technical report No. ARPA-17

THE MAGNETIC SCATTERING OF NEUTRONS BY NICKEL

By
Herbert A. Mook, Jr.

November 1965

DIVISION OF ENGINEERING AND APPLIED PHYSICS
HARVARD UNIVERSITY · CAMBRIDGE, MASSACHUSETTS

THE MAGNETIC SCATTERING OF NEUTRONS BY NICKEL

by

Herbert A. Mook, Jr.

Technical Report No. ARPA-17

Contract SD-88

November, 1965

Submitted to:

Advanced Research Projects Agency

The Department of Defense

Division of Engineering and Applied Physics

Harvard University

Cambridge, Massachusetts

BLANK PAGE

ABSTRACT

Despite the fact that a large amount of work has been devoted to understanding the nature of the electronic structure in the transition metals, very little precise knowledge of the magnetic electrons in the ferromagnetic metals is available. By using the neutron as a probe, precise information can be obtained about the spatial distribution of the magnetic moment density in a ferromagnet that is quite free of theoretical approximations. Neutron magnetic scattering amplitudes are generally quite small, especially at large scattering angles, and polarized neutron beams must be employed if accurate measurements are to be made. Professor C. G. Shull of M. I. T. has developed the polarized neutron beam technique to such an extent that extremely small magnetic scattering amplitudes can be measured with high precision. Professor Shull and his students have used the polarized beam technique to determine the magnetic form factors of iron and cobalt.

There are no accurate wavefunctions available for the magnetic electrons in a metal lattice; however, free atom wavefunctions are generally available for most transition metals. By comparison of the measured form factors with free atom form factors, and by direct calculation of the magnetic moment density from the measured neutron data, it was found that the magnetic moment distribution in iron and cobalt agreed with a model of the magnetization that imposed free atom-like distributions on a constant negative background. It was also discovered that the magnetic moment density was quite asymmetric about the nuclei in iron but almost spherical in cobalt. It was apparent that it would be valuable to know distribution of the magnetic moment density in nickel so that it could be compared with that of iron and cobalt. We thus decided to measure the magnetic form

factor of nickel. The measurements were performed at the M. I. T. reactor using one of Professor Shull's polarized beam spectrometers.

The magnetic scattering amplitude of nickel is smaller than that of either iron or cobalt and a large amount of neutron counting time was necessary to measure the desired number of reflections. It was also necessary to apply corrections to the neutron data. The data had to be corrected for incomplete polarization of the neutron beam and for the half-wavelength contamination of the beam. The polarization of the beam was close to 100% and the half-wavelength contamination was very small, otherwise these corrections could not be made with any certainty. Secondary extinction had to be minimized and the data corrected for any remaining secondary extinction that could not be eliminated. The data also had to be corrected for any multiple scattering effects that might be present. The magnetic scattering amplitude for nickel was determined for the first 27 Bragg reflections, corresponding to a $\frac{\sin \theta}{\lambda}$ value of 1.16.

The measured form factor for nickel was compared to free ion form factors that were available. It was discovered that the measured form factor agreed extremely well with an unrestricted Hartree Fock free ion form factor for $Ni^{\#}$ provided a uniform negative contribution was included in magnetization. The measured form factor is not a smooth function of $\frac{\sin \theta}{\lambda}$ showing that the magnetic moment distribution in nickel is very asymmetric about the nucleus. From the comparison of the measured and free ion form factors it was determined that 81 $\pm$ 1% of the 3d magnetic electrons occupy orbitals with t_{2g} symmetry compared to the 60% required for spherical symmetry. Shull's data show that 47% of the 3d electrons occupy t_{2g}

orbitals in iron. Thus, the magnetic moment density is spread out along the [111] direction in nickel and the [100] direction in iron relative to the other crystallographic directions.

The magnetic form factor was Fourier transformed to give a three-dimensional map of the magnetic moment density directly from the measured data. The map shows clearly the asymmetry in the magnetic moment distribution. The Fourier series from which the density map was obtained converges too slowly to give information about the moment density in the region far from the nickel nuclei. A Fourier series was derived that gives the magnetic moment density averaged in space over a cubic block. This series, giving the average density, converges very rapidly and it is found from it that the magnetic moment density goes negative in the region between the atoms. This is in agreement with the comparison between the free ion and measured form factors which requires that a uniform negative contribution be included in the magnetization. The size of the negative contribution agrees very closely in the two cases and the analysis of the data is consistent with a model of the magnetization which assigns the magnetic moment of nickel in the following way: 3d spin+0.656 μ_β; 3d orbit + 0.055 μ_β; uniform negative contribution -0.105 μ_β .

The neutron data give no information about the origin of the negative contribution. One possibility is that the 4s electron spins in the metal might be oppositely polarized to the 3d electron spins. 4s electron form factors fall to a very small value before the first Bragg reflection so the 4s electrons cannot be seen directly by the neutrons. Another possibility is that spin polarization effects in the 3d band may give an effective negative

contribution in the region between the atoms. In this case all the scattering would take place from the 3d band. Since a negative contribution to the magnetization is found in iron, cobalt, and nickel, it seems that the origin of the negative contribution must be intimately connected with the interaction that makes these materials ferromagnetic.

TABLE OF CONTENTS

TABLE OF CONTENTS (Continued)

LIST OF FIGURES

LIST OF TABLES

ACKNOWLEDGEMENTS

There are many people both at Harvard and M. I. T. who helped make possible the work described in this thesis

In particular, I would like to acknowledge the help and guidance given me by Professor R. V. Jones of Harvard and Professor C. G. Shull of M. I. T. It was Professor Jones who first interested me in the field of neutron diffraction and the many discussions with him during the course of the thesis work were sincerely appreciated. Professor Shull developed the technique that made the experimental work possible. He was very kind in giving me the complete use of his laboratory and experimental facilities. His many suggestions and his keen insight into the problems involved were of invaluable help.

I want to express my appreciation to the members of the Neutron Diffraction Group for their help. I particularly want to thank Walter Phillips, Alan Wedgwood, Stephen Spooner, and Yuji Ito for many helpful discussions and Armand D'Addario, our fine technician, for many valuable ideas and help in the shop.

A. J. Freeman supplied the free atom calculations and was the source of many helpful suggestions.

I would also like to thank R. J. Weiss of the Watertown Arsenal for help with the asymmetry analysis of the form factor and Professor H. Ehrenreich of Harvard University and his group for their interest in the problem, and their analysis of the form factor in terms of a band calculation for nickel metal.

BLANK PAGE

THE MAGNETIC SCATTERING OF NEUTRONS BY NICKEL

by

Herbert A. Mook
Division of Engineering and Applied Physics
Harvard University, Cambridge, Massachusetts

I. REVIEW OF THEOI Y AND EXPERIMENT

A. Introduction

When a neutron is scattered by a magnetic atom there are two main interactions that take place. There is a nuclear force interaction between the neutron and the nucleus of the scattering atom. For neutrons of thermal energy the neutron wavelength is very large compared to the nucleus and only the S partial wave is significant in the scattering interaction. This means nuclear scattering is independent of scattering angle. If the atom has any unpaired electrons there will also be an interaction between the magnetic moment of the neutron and the magnetic moment of the unpaired electrons. The thermal neutron wavelength is of the same order as the radial extent of the atomic electrons and one finds that the magnetic interaction between the atomic and neutron moments is strongly dependent on the scattering angle.

This reportdiscusses the measurement of the angular distribution of magnetic scattering in nickel metal. The magnetic scattering in nickel is very small in intensity, and the measurements were made by observing the interference term between the magnetic and nuclear scattering. We will see later how this can be

done by using polarized neutron beams. The angular distribution of the magnetic scattering is simply related to the spatial distribution of the periodic magnetic moment density in the scattering material. Sufficiently accurate measurements have been made that the magnetic moment density in nickel can be well determined in three dimensions.

In the iron series transition metals most of the magnetic moment density results from the 3d electronic shell. Despite the fact that a great deal of effort has been spent to gain an understanding of the behavior of the 3d electrons in the transition metals, very little is known about their exact nature. The neutron diffraction measurements give direct information about the 3d magnetic electrons that is quite free of theoretical approximations. It is unusual in the study of transition metals that precise experimental measurements have such a direct and meaningful interpretation.

The basic measurement of the magnetic scattering is fairly straightforward and is discussed in Chapter I. There are several small but fairly involved corrections that need to be made to obtain the final data and these are discussed in Chapter II. The results of the measurement and comparison with theory are discussed in Chapter III. If the reader is not concerned with the details of the experimental methods he may omit Chapter II and concern himself only with the review sections of Chapter I and the final results of Chapter III.

B. Magnetic Scattering

The theory of magnetic scattering was first developed by Schwinger [1]. The first comprehensive treatment of the scattering of polarized neutrons was developed by Halpern and Johnson [2] and their work has been extended by other authors to include orbital effects and higher-order terms [3-7]. The

deviation of magnetic scattering presented here follows that given by Blume [5] and Marshall [7].

The cross section in the Born approximation for a process in which the scattering system goes from state q to state q' while the neutron is scattered from wave vector $\bar{k}$ to $\bar{k}'$ and spin state S to S' is given by

$$\frac{d\sigma}{d\Omega'}_{qs\rightarrow q's'} = \frac{k'}{k}\left(\frac{m_o}{2\pi\hbar^2}\right)^2 \langle qs \mid U^{\dagger}(\bar{K}) \mid q's'\rangle\langle q's' \mid U(\bar{K})\mid qs\rangle \quad (1\text{-}1)$$

where $\bar{K} = \bar{k} - \bar{k}'$ and U (K) is the Fourier transform of the interaction between the neutron and the scatterer. $\bar{k}'$ is given by the energy conservation condition

$$\frac{\hbar^2 k'^2}{2m_o} + E_{q'} = \frac{\hbar^2 k^2}{2m_o} + E_q \quad (1\text{-}2)$$

To get the total cross section from (1-1) we must sum over the final states q's', and average over the initial states qs taking account of their different probabilities P_q and P_s. Usually P_q is given by the Boltzmann distribution

$$P_q = \frac{e^{-E_q/kT}}{\sum_q e^{-E_q/kT}} \quad (1\text{-}3)$$

Performing the summation and averaging processes and including relationship (1-2) we obtain

$$\frac{d^2\sigma}{d\Omega' dE'} = \sum_{qs} P_q P_s \sum_{q's'} \frac{k'}{k}\left(\frac{m_o}{2\pi\hbar^2}\right)^2 \langle qs \mid U^{\dagger}(\bar{K}) \mid q's'\rangle\langle q's' \mid U(\bar{K})\mid qs\rangle \times$$

$$\delta\left\{\frac{\hbar^2 k'^2}{2m_o} + E'_q - \frac{\hbar^2 k^2}{2m_o} - E_q\right\} \quad (1\text{-}4)$$

We would like to consider scattering of polarized neutron beams, and, in general, this cannot be done using a single wavefunction for the following reason. Choosing an arbitrary quantization axis, which we will call the z axis, the most general wavefunction describing the spin of a neutron is

$$\psi = a\alpha + b\beta \tag{1-5}$$

where α is the wavefunction representing spin up and β is the wavefunction representing spin down. If the wavefunction is normalized, a and b obey the equation

$$|a|^2 + |b|^2 = 1 \tag{1-6}$$

The expectation values of the x, y, and z spin components are given by

$$\begin{aligned} \tilde{S}_x &= 1/2\,[a^* b + b^* a] \\ \tilde{S}_y &= 1/2\; i\,[ab^* - a^* b] \\ \tilde{S}_z &= 1/2\,[\,|a|^2 - |b|^2] \end{aligned} \tag{1-7}$$

If we set b equal to zero, $\tilde{S}_x$ and $\tilde{S}_y$ would be zero and $\tilde{S}_z$ would be 1/2. The spin would then be completely polarized along the z axis. If a is zero, the spin is completely polarized along the -z axis. Other choices of a and b will give intermediate values of $\tilde{S}_z$ but must also give non-zero values for $\tilde{S}_x$ or $\tilde{S}_y$ or both. So for all other choices the spin is polarized along some direction other than the z axis, however, since from (1-7)

$$\tilde{S}_x^2 + \tilde{S}_y^2 + \tilde{S}_z^2 = 1/4\,[\,|a|^2 + |b|^2\,] = 1/4 \tag{1-8}$$

the spin must be completely polarized along some direction. Thus, no matter what choice is made for a and b, (1-5) always describes a spin completely polarized in one direction. We see then that in order to describe partially polarized or unpolarized beams we cannot use one wavefunction but must use an average over many wavefunctions. We could then treat the scattering of polarized beams in the following manner. Using (1-4) we could calculate cross sections for scattering out of initial state (1-5), treating a and b as arbitrary. The average over the initial wavefunctions could then be performed by aver-

aging the result over the magnitudes and relative phases of a and b. In fact, this turns out to be a very difficult process and it is much easier to do the calculation by introducing the concept of a density matrix.

We wish to find a shorthand way of describing the wavefunction (1-5) by specifying the values of a and b. This can be done by defining the density matrix

$$\rho = \begin{pmatrix} aa^* & b^*a \\ a^*b & bb^* \end{pmatrix} \tag{1-9}$$

Notice that

$$\mathrm{tr}\rho = aa^* + bb^* = 1 \tag{1-10}$$

Also, we can show by comparison with (1-7) that

$$\begin{aligned} \tilde{S}_x &= \mathrm{tr}[\sigma_x \rho] \\ \tilde{S}_y &= \mathrm{tr}\,[\sigma_y \rho] \\ \tilde{S}_z &= \mathrm{tr}\,[\sigma_z \rho] \end{aligned} \tag{1-11}$$

where σ_x, σ_y and σ_z are the Pauli spin operators. All the initial wavefunctions can be averaged over by simply averaging over the elements of (1-9) to give the density matrix for the whole beam

$$\rho = \begin{pmatrix} \widetilde{aa^*} & \widetilde{b^*a} \\ \widetilde{a^*b} & \widetilde{b^*b} \end{pmatrix} \tag{1-12}$$

Then (1-11) is still correct if $\tilde{S}_a$ is reinterpreted as the expectation value of $\tilde{S}_a$ averaged over the whole neutron beam. Because ρ is a two-by-two matrix, it can be expressed as a linear combination of the four linearly independent two- two matrices which are the unit matrix and the three Pauli spin matrices.

$$\rho = g + P_x\sigma_x + P_y\sigma_y + P_z\sigma_z$$

$$= \begin{pmatrix} g + 1/2\ P_z & 1/2(P_x - iP_y) \\ 1/2(P_x+iP_y) & g-1/2\ P_z \end{pmatrix} \tag{1-13}$$

g, P_x, P_y, and P_z are constants and have to be determined. We can find g immediately since by (1-10) $tr\rho = 2g = 1$.

The other constants can be found using (1-11).

$$\overset{\leftrightarrow}{S}^z = tr(\sigma_z\rho) = g\ tr\ \sigma_z + P_x\ tr\ \sigma_z\sigma_x + P_y\ tr\ \sigma_z\sigma_y + P_z tr\ \sigma_z^{\,2} \tag{1-14}$$

Now $tr\sigma_z$, $tr\sigma_z\sigma_x$, $tr\sigma_z\sigma_y$ are all zero and $tr\ \sigma_z^{\,2} = 1/2$. Thus (1-14) becomes

$$\overset{\leftrightarrow}{S}^z = 1/2P_z \tag{1-15}$$

P_z is therefore the z component of the polarization. Similar equations hold for the other components; thus, the vector $\bar{P}$ defined by the components P_x, P_y, P_z denotes the polarization of the beam. (1-13) then becomes

$$\rho = 1/2\ \bar{1} + \bar{P}\cdot\bar{S} \tag{1-16}$$

Now let us go back and consider our formula for the cross section (1-4). We want to concentrate on the neutron spin, so let us suppose the sums over q' and q have been done giving

$$\frac{d\sigma^2}{d\Omega dE} \approx \sum_s P_s \sum_{s'} \langle S \mid \bar{O}^{\dagger} \mid S' \rangle\langle S' \mid \bar{O} \mid S \rangle \tag{1-17}$$

where $\bar{O}$ is a suitably defined operator. The sum over S' can be done immediately giving

$$\frac{d\sigma^2}{d\Omega dE} \approx \sum_s P_s \langle S \mid \bar{O}^{\dagger}\bar{O} \mid S \rangle \tag{1-18}$$

The above expressions for the cross section are only useful when there is no phase correction between the states with quantum number S; i.e., the densi-

ty matrix is diagonal with respect to the states S. In this case, the probability P_s is just the diagonal element $\langle S|\rho|S\rangle$ and (1-18) can be written

$$\frac{d^2\sigma}{d\Omega dE} \approx \sum_s \langle S | \bar{O}^\dagger \bar{O} | S\rangle\langle S | \rho | S\rangle \tag{1-19}$$

If ρ is diagonal $\langle S' | \rho | S\rangle \delta_{ss'} = \langle S | \rho | S\rangle$ so (1-19) can be written

$$\frac{d^2\sigma}{d\Omega dE} \approx \sum_{ss'} \langle S | \bar{O}^\dagger \bar{O} | S'\rangle\langle S' | \rho | S\rangle \tag{1-20}$$

and this can be summed immediately over S' giving

$$\frac{d\sigma^2}{d\Omega dE} \approx \sum_s \langle S | \bar{O}^\dagger \bar{O}\, \rho | S\rangle = \mathrm{tr}\,(\bar{O}\bar{O}^\dagger \rho) \tag{1-21}$$

The last form is independent of the representation used to label the states S and thus in this last form it does not matter whether or not ρ is diagonal. A formula that is more general than (1-4) and includes the effects of neutron polarization can therefore be written in the following way

$$\frac{d^2\sigma}{d\Omega' dE'} = \sum_{qq'} P_q \frac{k'}{k}\left(\frac{m_o}{2\pi\hbar^2}\right)^2 \mathrm{tr}\left[\langle q | U^\dagger(\bar{K}) | q'\rangle\langle q' | U(\bar{K}) | q\rangle \rho\right]$$
$$\times\, \delta\left[\frac{\hbar^2}{2m_o}(k'^2 - k^2) + E_q' - E_q\right] \tag{1-22}$$

where the trace is to be taken only with respect to the neutron spin coordinates.

The interaction between the neutron and the scattering system is usually broken up into an interaction with the nuclei of the scatter U_n and a magnetic interaction U_m with the spin and orbital moments of the electrons. U_n and U_m have been given by Halpern and Johnson [2] and are

$$U_n(\bar{K}) = \frac{2\pi\hbar^2}{m_o} \sum_{\bar{n}j} e^{i\bar{K}\cdot(\bar{n}+\bar{d}_j)} a_{\bar{n}j} = \frac{2\pi\hbar^2}{m_o} T$$

$$U_m(\bar{K}) = \frac{2\pi\hbar^2}{m_o} \frac{2\gamma e^2}{mc^2} \sum_i e^{i\bar{K}\cdot\bar{r}_i} [\hat{K} \times (\bar{S}_i \times \hat{K}) - \frac{i}{K} (\hat{K} \times \bar{p}_i)] \cdot \bar{S}$$

$$= \frac{4\pi\hbar^2 \gamma e^2}{m_o mc^2} \bar{S} \cdot \bar{Q} \qquad (1\text{-}23)$$

where $\bar{n} + \bar{d}_j$ is the position of the scattering nucleus, $\bar{n}$ giving the position of the unit cell and $\bar{d}_j$ the position vector of the nucleus within the unit cell. $\bar{r}_i$, $\bar{S}_i$, p_i and m are, respectively, the position, spin, momentum, and mass of the i th electron. S is the neutron spin, $\gamma = 1.191$ is the neutron gyromagnetic ratio and $a_{\bar{n}j}$ is the neutron scattering length. To find the cross section we must substitute (1-23) in (1-22) and perform the required traces. It is helpful to remember that

$$S_\alpha S_\beta = 1/4 \ \delta_{\alpha\beta} + 1/2 \ i \ \varepsilon_{\alpha\beta\gamma} S_\gamma \qquad (1\text{-}24)$$

where α β γ run over x y z and $\varepsilon_{\alpha\beta\gamma}$ is zero unless α, β and γ are all different, plus unity if $\alpha\beta\gamma$ are in cyclic order and minus unity if $\alpha\beta\gamma$ are not in cyclic order. Using (1-24) it is easy to show

$$\text{tr } \bar{1} = 2 \qquad \text{tr } S_\alpha S_\beta = 1/2 \ \delta_{\alpha\beta}$$

$$\text{tr } S_\alpha = 0 \qquad \text{tr } S_\alpha S_\beta S_\gamma = 1/4 \ i\varepsilon_{\alpha\beta\gamma} \qquad (1\text{-}25)$$

Substituting (1-23) in (1-22) and using (1-25) we obtain

$$\frac{d^2\sigma}{d\Omega' dE'} = \frac{k'}{k} \sum_{qq'} p_q \left[\langle q|T^\dagger|q'\rangle\langle q'|T|q\rangle + \left(\frac{\gamma e^2}{mc^2}\right) \langle q|T^\dagger|q'\rangle\langle q'|\bar{P}\cdot\bar{Q}|q\rangle + \right.$$

$$\left(\frac{\gamma e^2}{mc^2}\right) \langle q|\bar{P}\cdot\bar{Q}^\dagger|q'\rangle\langle q'|T|q\rangle + \left(\frac{\gamma e^2}{mc^2}\right)^2 \langle q|\bar{Q}^\dagger|q'\rangle\cdot\langle q'|\bar{Q}|q\rangle +$$

$$\left. i\left(\frac{\gamma e^2}{mc^2}\right)^2 \bar{P}\cdot(\langle q|\bar{Q}^\dagger|q'\rangle \times \langle q'|\bar{Q}|q\rangle)\right] \times$$

$$\delta\left(\frac{\hbar^2}{2m_o}(k'^2 - k^2) + E_{q'} - E_q\right) . \qquad (1\text{-}26)$$

In deriving (1-26) we have used the relation

$$(\bar{A}\times\bar{B})^\alpha = \sum_{\beta\gamma} \varepsilon_{\alpha\beta\gamma} A^\beta B^\gamma$$

for the components of the vector product of two vectors $\bar{A}$ and $\bar{B}$.

It is generally assumed that the electron distribution responds so quickly to the motion of the nuclei that the Debye-Waller temperature factors for nuclear and magnetic scattering are the same. We will see later that this assumption is well supported by experimental evidence. The quantity measured in the nickel-scattering experiments is the ratio of the magnetic to the nuclear scattering. In this case, the Debye-Waller temperature factors will cancel in the final result and we might as well drop them at this time. We can thus assume that the nuclei are rigidly fixed and ignore lattice vibrations. We are only interested in elastic scattering, so we can take $|q'\rangle = |q\rangle$. It is much easier at this point to assume the orbital moment is quenched. This is very nearly true in nickel although when the magnetic form factor is compared with theoretical calculations we will want to include the orbital term. For convenience we will drop the orbital contribution at this time and quote the result complete with orbital term when we need it.

Using the above simplifications we can take over Halpern and Johnson's [2] result

$$\langle q|\bar{Q}|q\rangle = \sum_{\bar{n}j} e^{i\,\bar{K}\cdot(\bar{n}+\bar{d}_j)}\, \underline{f}_{nj}(\bar{K})\, \langle q|\hat{K}\times(\underline{S}_{nj}\times\hat{K})\,|\,q\rangle \qquad (1\text{-}27)$$

$\underline{S}_{nj}$ is the spin operator for the ion at the site $(\bar{n}, j)$ while $\underline{f}_{nj}(\bar{K})$ is the Fourier transform of that ion's spin density and is called the form factor for that ion. Since the Curie point of nickel is 631° [8], we can assume that only the ground state of the spin system is appreciably occupied so that

$$\langle q|\underline{S}_{nj}|q\rangle = S_{nj}\,\underline{\bar{\eta}}_{nj} \qquad (1\text{-}28)$$

where S_{nj} is the magnitude of the spin and $\underline{\bar{\eta}}_{nj}$ is a unit vector in the direction of the spin.

Since natural nickel is made up of three isotopes with different scattering amplitudes, we must average our scattering expressions over the isotope distribution found in natural nickel. Let

$$\langle a\rangle = \sum_{\alpha} C_\alpha a_\alpha \qquad (1\text{-}29)$$

where C_α is the concentration of the αth isotope and a_α is the scattering length for this isotope. Assuming the isotopes are randomly distributed

$$\langle \underline{a}_{nj}\rangle\langle \underline{a}_{nj}\rangle = \langle a_j\rangle\langle a_j\rangle = |\langle a\rangle|^2 \text{ for } n \neq n' \;\; j \neq j'$$

$$= \langle |a_j|^2\rangle \text{ for } n = n' \;\; j = j'$$

$$\text{or } \langle \underline{a}_{nj}\rangle\langle \underline{a}_{n'j'}\rangle = |\langle a_j\rangle|^2 + (\langle |a_j|^2\rangle - |\langle a_j\rangle|^2)\,\delta_{\bar{n}\bar{n}'}\,\delta_{jj'} \qquad (1\text{-}30)$$

Substituting (1-27) in (1-26) and using (1-28) and (1-30) the elastic scattering cross section becomes

$$\frac{d\sigma}{d\Omega} = \left| \sum_{\bar{n}} e^{i\bar{K}\cdot\bar{n}} \right|^2 |F_N(\bar{K})|^2 + N \sum_j (\langle |a_j|^2 \rangle - |\langle a_j \rangle|^2) +$$

$$\frac{\gamma e^2}{mc^2} \sum_{\bar{n}j\,\bar{n}'j'} e^{i\bar{K}\cdot(\bar{R}_{\bar{n}j} - \bar{R}_{\bar{n}'j'})} \left[|\langle a_{j'} \rangle| f_{\bar{n}j}(\bar{K}) S_{\bar{n}j} \bar{P} \cdot \bar{q}_{\bar{n}j} + \right.$$

$$\left. |\langle a_j \rangle| f_{\bar{n}'j'}(\bar{K}) S_{\bar{n}j'} \bar{P} \cdot \bar{q}_{\bar{n}'j'} \right] + \left(\frac{\gamma e^2}{mc^2} \right)^2 \sum_{nj\,n'j'} e^{i\bar{K}\cdot(\bar{R}_{\bar{n}j} - \bar{R}_{\bar{n}'j'})} \times$$

$$S_{\bar{n}j} S_{\bar{n}'j'} f_{\bar{n}j}(K) f_{\bar{n}'j'}(\bar{K}) \left(\bar{q}_{\bar{n}'j'} \cdot \bar{q}_{\bar{n}j} + i\bar{P} \cdot (\bar{q}_{\bar{n}'j'} \times \bar{q}_{\bar{n}j}) \right) \qquad (1\text{-}31)$$

where we have defined

$$\bar{q}_{\bar{n}j} = \hat{K} \times (\bar{\eta}_{\bar{n}j} \times \hat{K}) \qquad (1\text{-}32)$$

and let $R_{\bar{n}j} = \bar{n} + \bar{d}_j$. In (1-31) $F_N(\bar{K}) = \sum_j e^{i\bar{K}\cdot\bar{d}_j} \langle a_j \rangle$ is the nuclear structure factor.

In a ferromagnet like nickel we are able to simplify equation (1-31) greatly by lining up all the spins in the sample with a large magnetic field. In this case, all the spins would be along the vector $\bar{\eta}$ so $\bar{q}_{\bar{n}j}$ would be independent of $\bar{n}$ and $\bar{j}$. We will see later that the experimental results are very easy to interpret if the magnetic field is applied perpendicular to the plate of scatter-

ing defined by k and k'. Taking then q_{nj} to be independent of n and j, the cross section reduces to

$$\frac{d\sigma}{d\Omega'} = \left| \sum_{\bar{n}} e^{i \bar{K} \cdot \bar{n}} \right|^2 \left\{ |F_N(\bar{K})|^2 + \frac{2\gamma e^2}{mc^2} S F_N(\bar{K}) F_M(\bar{K}) \bar{P} \cdot \bar{q} + \left(\frac{\gamma e^2}{mc^2} \right)^2 S^2 |F_M(\bar{K}) f(\bar{K})|^2 q^2 \right\} + N \sum_j \left(|\langle a_j \rangle^2| - |\langle a_j \rangle|^2 \right) \quad (1\text{-}33)$$

where $F_M(\bar{K}) = \sum_j e^{i \bar{K} \cdot \bar{d}_j}$ is the magnetic structure factor for a ferromagnet.

Let us now consider the sum $\sum_{\bar{n}} e^{i \bar{K} \cdot \bar{n}}$. This sum contains N terms

where N is the number of lattice points in the crystal. For most values of $\bar{K}$ these terms will have different phases both positive and negative, so there will be a great deal of cancellation and the sum will be negligible.

For certain values of $\bar{K}$, however, all the terms will have zero phase and the sum will be N. If we define a reciprocal lattice vector $\bar{\tau}$ by

$$e^{2\pi i \bar{\tau} \cdot \bar{n}} = 1 \quad \text{for all } \bar{n}, \quad (1\text{-}34)$$

then whenever $\bar{K}$ is equal to 2π times a reciprocal lattice vector $\bar{\tau}$ the sum is N, and as $\bar{K}$ moves slightly from $2\pi\bar{\tau}$ the sum falls rapidly to zero. After some consideration of the volume under this very narrow peak, one finds

$$\left| \sum_{\bar{n}} e^{i \bar{K} \cdot \bar{n}} \right|^2 = \frac{N(2\pi)^3}{V_o} \sum_{\bar{\tau}} \delta(\bar{K} - 2\pi \bar{\tau}) \quad (1\text{-}35)$$

where V_o is the unit cell volume. This expression shows that the first set of terms in equation (1-33) will only make a contribution when $\bar{K}$ is equal to 2π times a reciprocal lattice vector or that the scattering will all fall in certain

Bragg peaks. These terms then give the coherent Bragg scattering. The scattering resulting from the last term of equation (1-33) is found uniformly everywhere and is called the diffuse scattering. When the conditions are such that Bragg coherent scattering may take place, one finds that the coherent scattering is much larger than the diffuse scattering and that the diffuse scattering only comes in as a small correction to the coherent scattering.

For a face-centered cube,

$$\sum_j e^{i \bar{K} \cdot \bar{d}_j} = \sum_j e^{2\pi i (hx_j + ky_j + \ell z_j)} = \begin{cases} 0 \text{ for } h, k, \ell \text{ mixed} \\ 4 \text{ for } h, k, \ell \text{ All odd or All even} \end{cases} \quad (1\text{-}36)$$

Thus we have for the coherent scattering

$$\frac{d\sigma}{d\Omega} = \frac{4N(2\pi)^3}{V_o} \left[| \langle a \rangle |^2 + | \langle a \rangle | \frac{2\gamma e^2}{mc^2} S f(\bar{K}) \bar{P} \cdot \bar{q} + \left(\frac{\gamma e^2}{mc^2} \right)^2 S^2 f^2(\bar{K}) q^2 \right] \quad (1\text{-}37)$$

One usually calls $\frac{\gamma e^2}{mc^2} Sf(\bar{K})$ the magnetic scattering amplitude and denotes it by p. p is a function of scattering angle through the form factor $f(\bar{K})$ which is 1 when $\bar{K} = 0$ and falls off from 1 when $(\bar{K})$ differs from zero. $| \langle a \rangle |$ is called the nuclear scattering amplitude and is usually denoted by the letter b. b is independent of the scattering angle. Thus, finally, we may write for the coherent cross section:

$$\frac{d\sigma}{d\Omega} = \frac{4N(2\pi)^3}{V_o} (b^2 + 2 pb \bar{P} \cdot \bar{q} + p^2 q^2) \quad (1\text{-}38)$$

This expression gives the cross section for the scattering of a polarized neutron beam by a magnetic material with no orbital moment, completely saturated

in a high magnetic field. This is very nearly the case for nickel under the experimental conditions used and frequent use will be made of expression (1-38).

C. MAGNETIC FORM FACTORS

As mentioned in the introduction, the angular distribution of the magnetic scattering is related directly to the distribution of magnetic moment density of the scattering atom. The angular distribution of the magnetic scattering is given by the form factor and we define the form factor as the Fourier transform of the spatial distribution of the magnetic moment density. As we shall see in the next section, polarized neutron beams are needed for accurate form factor measurements. The first accurate polarized beam magnetic form factor measurement were made by Nathans, Shull, Shirane and Andresen [9] on iron and nickel. Since then, a number of form factor measurements have been reported [10-14]. The most interesting of these to compare with nickel are the very complete measurements of Shull and Yamada [10] on iron, and Moon [11] on hexagonal cobalt. In both iron and cobalt very good agreement was obtained between the measured values and free atom form factors. The form factors were unrestricted Hartree-Fock calculations that allowed electrons in the same atomic shell, but having different spins, to have different radial distributions. In both iron and cobalt this very good agreement was obtained by assuming the spin density was the sum of an aspherical 3d contribution and a negative constant. We shall see later that this same assumption is employed in nickel to give good agreement with calculated results.

The behavior of the magnetic electrons in the transition metals is a difficult problem [15, 16]. It is somewhat surprising that free atom form factors should agree with the measured values for a metal so closely. The rea-

son that free atom form factors are any good for a metal at all seems to stem from the fact that the 3d wavefunctions at the top of the band in the metal are not much different from the free atom wavefunctions [17, 18, 19]. The wavefunctions at the bottom of the 3d band are quite diffuse compared with free atom wavefunctions, and neutrons can be scattered by the difference in radial distributions of spin up and spin down electrons at the bottom of the band even without a net spin difference. An unrestricted Hartree-Fock calculation by Freeman and Watson [20] shows that there is a small but noticeable difference in the radial distribution for spin up and spin down electrons in the free atom. This difference may be larger in a metal but it is expected that most of the scattering must come from the unpaired spins at the Fermi level near the top of the band where the free atom and metal 3d wavefunctions are in substantial agreement.

The neutron magnetic form factor is dependent on the difference in the radial distribution of spin up and spin down electrons and is different from a form factor derived from any single electron of either type [20]. The neutron form factor is expanded in relation to any of the 3d electron X-ray form factors representative of the charge distribution. For this reason, we cannot use neutron form factor data to get an accurate picture of the 3d electron charge distribution, which will be different from the magnetic moment distribution of the atom.

Shull and Yamada [10] found that in iron the 3d electron spin distribution was quite aspherical about the nucleus as the form factor at a given scattering angle and wavelength was dependent on the direction of scattering through the crystal. Moon [11], however, found the spin distribution to be quite spherical in hexagonal cobalt. In a cubic field the degenerate d orbitals split into triply degenerate t_{2g} and doubly degenerate e_g orbitals. The t_{2g}

orbitals are peaked along the cube body diagonal while the e_g orbitals are peaked along the cube edges. Shull and Yamada found that in iron 47 % of the magnetic electrons had t_{2g} symmetry and 53 % had e_g symmetry rather than the 60 % and 40% required for spherical symmetry. The data of Nathans et al. [9] for the magnetic scattering in nickel did not go far enough out in angle to determine the asymmetry of the magnetic electron distribution. One of the objectives of this study of nickel was to see how the asymmetry in the magnetic electron distribution compares with that of iron and hexagonal cobalt.

D. EXPERIMENTAL METHODS

The quantity that we wish to measure is the magnetic scattering amplitude p because the form factor is determined from the angular dependence of p. If a polarized neutron beam is not available, one can consider the following experiment. Apply a strong magnetic field perpendicular to the scattering vector $\bar{K}$ so that $\bar{q}$ becomes a unit vector in the direction of the magnetic field. From expression (1-38) the cross section becomes proportional to b^2+p^2 since the $\bar{P}\cdot\bar{q}$ term will average to zero for an unpolarized beam. One then applies a strong magnetic field along the vector $\bar{K}$ making $q=0$ and the cross section will be proportional to b^2. Assume the sample crystal introduces no corrections into the data. Then if we bring a beam of monochromatic neutrons onto the sample crystal, the ratio of the scattered intensities in the two cases for a coherent Bragg peak will be equal to the ratio of the cross sections or

$$R = \frac{b^2+p^2}{b^2} \quad . \tag{1-39}$$

At the first Bragg peak, p for nickel is about $.12 \times 10^{-12}$ cm and 1.03×10^{-12} cm is the accepted value for b [21]. R then becomes

$$R = \frac{(1.03)^2 + (.12)^2}{(1.03)^2} \sim 1.013$$

This gives only about a 1.5% effect for the first Bragg peak in nickel and it would be difficult to determine the magnetic scattering amplitude for many reflections in the above manner. Since, in fact, this is the best experiment that can be done with unpolarized neutrons, polarized neutron beams must be employed to make the experiment feasible.

Polarized neutrons can be produced by using a monochromating crystal with equal nuclear and magnetic scattering amplitudes at the monochromating reflection used. If there is an upward magnetic field on the monochromating crystal, the cross section for neutrons of spin up will be proportional to $(b + p)^2 = (2b)^2$ under the above conditions, while the cross section for spin down neutrons will be $(b-p)^2 = 0$. The monochromater-polarizer used in the nickel measurements was a disorder alloy crystal of $Co_{.92}Fe_{.08}$ placed in a magnetic field of about 3000 oersteds. The (200) reflection of this crystal was used for which b is very nearly equal to p and the polarization was very close to 100% .

The general experimental arrangement is similar to that used by Nathans et al.[9]. A diagram of the M. I. T. S-4 polarized beam spectrometer is shown in Fig. 1. A guide field of about 150oe. parallel to the direction of the neutron polarization is maintained along the path between the polarizing crystal and the sample crystal. The sample is positioned in a magnet producing a field of about 7200oe. in the same direction as the guide fields and the initial neutron polarization direction. A solenoid is placed in the path between

BLANK PAGE

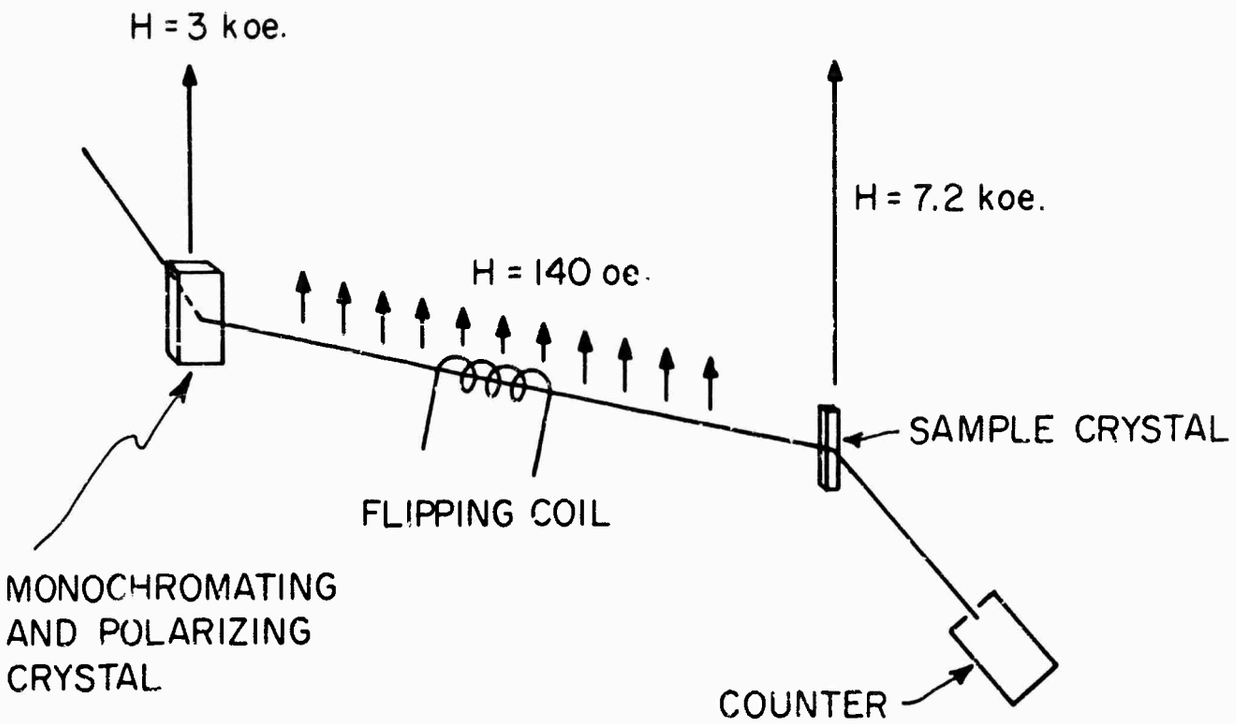

FIG. 1 EXPERIMENTAL ARRANGEMENT

the polarizing crystal and the sample so that the polarized neutron beam can pass along its axis. The solenoid can be energized with R. F. current that produces an R. F. field perpendicular to the constant guide field. When the R. F. frequency of the solenoid is set to match the energy level separation of the two spin states in the guide field, transitions are induced between the two spin states. If the current in the R. F. solenoid is then adjusted to match the neutron transit time in the solenoid the neutrons passing through the solenoid are flipped over from spin up to spin down with a probability very close to one. Thus, by energizing the solenoid, neutrons polarized downward are brought onto the sample.

The experiment can then be done in the following manner. The sample crystal is positioned at a Bragg peak and the scattering from the sample of spin up neutrons is counted for an interval of time, usually about ten minutes in practice. The cross section for spin up neutrons is proportional to $(b+p)^2$. The R. F. solenoid, usually called the flipper, is then turned on and the scattering of spin down neutrons is counted for an equal interval of time. The cross section for spin down neutrons is proportional to $(b-p)^2$. Assuming that the sample crystal is ideal and that the beam polarization is perfect, the ratio of the intensity of the spin up neutrons scattered to the spin down neutrons scattered is given by

$$R = \frac{(b+p)^2}{(b-p)^2} \qquad (1\text{-}40)$$

Putting in numbers again for the first Bragg reflection we get

$$R = \frac{(1.03 + .12)^2}{(1.03 - .12)^2} = 1.597$$

and this is nearly a 60% intensity effect. The experiment then consists of measuring R, and p is obtained from equation (1-40). R can be measured accurately for a large number of reflections and in each case the magnetic

scattering amplitude is given by (1-40) since b is a constant independent of angle.

For the actual experiment there are two separate counting channels. One of these systems, called the monitor channel, receives pulses from a low efficiency counter mounted directly in the beam incident on the sample crystal. The main counting channel counts for a preset number of monitor channel counts and prints the result by means of a digital recorder. By this arrangement small changes in the incident beam flux are cancelled out to first order. The flipper is turned on automatically in alternate counting periods. Scattering data for both spin up and spin down neutrons can thus be automatically collected as long as necessary to gain the desired counting statistics. Standard BF_3 proportional counters are used in both channels and standard commercial amplifiers and scalers are used in the counting circuits.

BLANK PAGE

II. CORRECTIONS TO THE EXPERIMENTAL DATA

A. Instrumental Corrections

In the ideal case where no corrections to the experimental data are necessary, the flipping ratio is given by

$$R = \frac{\int I_o g_o^+ \, d\lambda d\psi}{\int I_o g_o^- \, d\lambda d\psi} = \left(\frac{p+b}{p-b} \right)^2 \qquad (2\text{-}1)$$

where the integration is to be taken over all wavelengths λ and directions ψ of the beam I_o incident upon the crystal. g_o^+ and g_o^- are the ideal reflectivities of the sample crystal for spin up and spin down neutrons. For the ideal case considered above, the effects of incident beam divergence and wavelength spread cancel in the flipping ratio and R becomes proportional to the ratio of the cross sections for spin up and spin down neutrons given in (1-38).

Unfortunately, the ideal case is seldom realized in practice and there are corrections to the data that need to be made particularly for the first few reflections. The corrections to be considered in this section are characteristic of the particular spectrometer used for the experiment. Instrumental corrections must be made for imperfect beam polarization from the monochromating crystal, depolarization effects along the neutron path, imperfect spin flipping by the flipper, and half wavelength contributions in the beam. The polarization of the S-4 spectrometer is close to 100% and the half wavelength contamination is small; otherwise, these corrections could not be considered with any certainty. The derivation for the polarization corrections that follow is similar to that developed in previous work in the neutron diffraction laboratory and discussed, for instance, by Phillips [13].

In the actual experiment, the crystal is quite small and we can assume that the beam is uniform in intensity over the crystal and that the distribution of λ and ψ is the same in the beams polarized with spin up and spin down. Let P_o be the beam polarization just as the beam enters the sample crystal. Any magnetic field components not parallel to the neutron polarization direction will serve to depolarize the beam; thus, as we shall see later, in some cases, the neutron polarization in the sample can be smaller than the incident polarization P_o. Let the beam polarization in the sample crystal be given by P where P is defined by

$$P = \frac{I^+ - I^-}{I^+ + I^-} \qquad I^+ + I^- = I \tag{2-2}$$

where I^+ and I^- are the intensities of spin up and spin down neutrons in the sample crystal. One can then write

$$I^+ = I/2\,(1 + P)$$
$$I^- = I/2\,(1 - P) \tag{2-3}$$

If the efficiency of the flipper is given by f, the beam emerging from the flipper is characterized by

$$I_f^+ = (1-f)\, I_o^+ + f I_o^-$$
$$I_f^- = f I_o^+ + (1-f)\, I_o^- \tag{2-4}$$

I_f^+ and I_f^- are the intensities of spin up and spin down neutrons after passing through the flipper and I_o^+ and I_o^- are the corresponding initial intensities. The polarization of the beam emerging from the flipper is defined by

$$P_f = \frac{I_f^+ - I_f^-}{I_f^+ + I_f^-} \tag{2-5}$$

The measured polarization ratio using the flipper is then given by

$$R_{m_f} = \frac{\int [I^+(\lambda\psi)\, g_o^+(\lambda\psi) + I^-(\lambda\psi)\, g_o^-(\lambda\psi)]\, d\lambda\, d\psi}{\int [I_f^+(\lambda\psi)\, g_o^+(\lambda\psi) + I_f^-(\lambda\psi)\, g_o^-(\lambda\psi)]\, d\lambda\, d\psi} \quad . \tag{2-6}$$

The monochromating crystal which is positioned to scatter neutrons with wavelength λ at the (200) reflection will also scatter neutrons with wavelength $\lambda/2$ by means of the (400) reflection. The value of λ is chosen to be close to the peak of the Maxwell distribution of neutron wavelengths incident on the monochromating crystal. The half wavelength intensity is then quite far down on the Maxwell distribution curve so that

$$\frac{I_{\lambda/2}}{I_\lambda} << 1 \tag{2-7}$$

Then making use of the fact that

$$P_f = P_o\,(1-2f) \tag{2-8}$$

and including half wavelength terms, the measured flipping ratio is given by

$$R_{rm} = \frac{(1+P)\, g^+ + (1-P)\, g^- + \frac{I_{\lambda/2}}{I_\lambda}\, [(1+P_{\lambda/2})\, g^+_{\lambda/2} + (1-P_{\lambda/2})\, g^-_{\lambda/2}\,]}{[1+(1-2f)\,P]\, g^+ + [1-(1-2f)\,P]\, g^- + \frac{I_{\lambda/2}}{I_\lambda}\, [1+(1-2f_{\lambda/2})\,P_{\lambda/2}]\, g^+_{\lambda/2} + [1-(1-2f_{\lambda/2})\,P_{\lambda/2}]\, g^-_{\lambda/2}} \tag{2-9}$$

where g^+ and g^- are the acual crystal reflectivity functions for spin up and spin down neutrons averaged over the crystal volume. In the above equation the integration over the wavelength spread and beam divergence is not explicitly written. This integration must be carried out by using the crystal reflectivity

function, which we will consider in the next section, and using the above-mentioned assumptions regarding the equality of the beam distribution over the crystal for spin up and spin down incident neutron intensities. Since any corrections to the data are very small, this procedure is well justified for finding polarization correction expressions.

The polarization is quite high and the flipping efficiency is near 100%, so P is only slightly smaller than 1 and (1-2f)P is slightly more positive than -1. We can, therefore, expand Eq. (2-9) about small deviations ξ and η in the beam polarization. Let

$$\begin{aligned} P &= 1 - \xi \\ (1-2f)\,P &= -1 + \eta \end{aligned} \qquad (2\text{-}10)$$

and substitute (2-10) into (2-9) giving

$$R_m = \frac{g^+ - \xi/2\,(g^+ - g^-) + \dfrac{I_{\lambda/2}}{I_\lambda}\, g_{\lambda/2}}{g^- + \eta/2\,(g^+ - g^-) + \dfrac{I_{\lambda/2}}{I_\lambda}\, g_{\lambda/2}} \qquad (2\text{-}11)$$

where we have assumed $g^+_{\lambda/2} = g^-_{\lambda/2} = g_{\lambda/2}$ in the half wavelength term. This is certainly valid in the case of nickel considering that the half wavelength term is very small. Since η and $\dfrac{I_{\lambda/2}}{I_\lambda}$ are small we can expand the denominator of Eq. (2-11) giving to first order

$$R_m = \frac{g^+}{g^-} - \xi/2\,\frac{g^+ - g^-}{g^-} - \eta/2\,\frac{g^+}{g^-}\left(\frac{g^+ - g^-}{g^-}\right) + \frac{I_{\lambda/2}}{I_\lambda}\,\frac{g_{\lambda/2}}{g^-}\left(1 - \frac{g^+}{g^-}\right) \qquad (2\text{-}12)$$

Let $R_{ext.} = \dfrac{g^+}{g^-}$ which is the measured flipping ratio when P = 1 and f = 100% but crystal extinction may be present. Then

$$R_m = R_{ext.} - \xi/2\,(R_{ext.}-1) - \eta/2\,R_{ext.}\,(R_{ext.}-1) + \frac{I_{\lambda/2}}{I_\lambda}\,\frac{g_{\lambda/2}}{g^-}\,(1-R_{ext.}) \qquad (2\text{-}13)$$

Since the correction terms are small, R_m does not differ much from $R_{ext.}$ and we can write

$$R_{ext.} = R_m + \xi/2\,(R_m-1) + \eta/2\,R_m(R_m-1) + \frac{I_{\lambda/2}}{I_\lambda}\,\frac{g_{\lambda/2}}{g^-}\,(R_m-1) \qquad (2\text{-}14)$$

or using (2-10)

$$R_{ext.} = R_m + (R_m-1)\left\{1/2\,(1-P) + 1/2\,[\,(1-2f)\,P+1]\,R_m + \frac{I_{\lambda/2}}{I_\lambda}\,\frac{g_{\lambda/2}}{g^-}\right\} \qquad (2\text{-}15)$$

The determination of P, f and $I_{\lambda/2}$ are discussed in Appendix A. Once these are known, (2-15) may be used to correct the flipping ratio for incomplete polarization and half wavelength effects. The flipping ratio $R_{ext.}$ still includes extinction effects, however, so we will consider extinction corrections in the next section.

B. Extinction

In the last section we have dealt with the corrections made necessary by the properties of the polarized beam spectrometer itself. In this section, we will consider the problem of primary and secondary extinction which depends on the properties of the sample crystal. For neutron scattering, secondary extinction is much more important than primary extinction so we will deal with it first.

1. Secondary Extinction

Secondary extinction was first treated theoretically by Darwin [22] and later applied particularly to neutron scattering by Bacon and Lowde [23] and

Moon [11]. The treatment here will follow that given by Bacon and Moon. We make the assumption, first proposed by Darwin, that the sample crystal consists of a large number of small perfect crystal blocks, called mosaic blocks, that are tipped slightly in angle relative to one another. In this case, Bragg reflection occurs in each block and the total intensity is obtained by summing up the intensities from each block. Secondary extinction results from the reduction in beam strength seen by those blocks deep in the sample relative to those blocks near the surface where the neutron beam enters. Simultaneous differential equations can be set up for the transmitted and reflected beams in each block and solved to get the total reflected intensity. If there were no extinction, the reflectivity would be given by

$$g_o^{\pm} = \int Q^{\pm} W(\theta_\beta - \phi)\, t d\phi \qquad (2\text{-}16)$$

where $Q^{\pm} = \dfrac{\lambda^3 N^2 F^{2\pm}}{\sin^2 \theta_\beta}$ and $W(\theta_\beta - \phi)$ is a function normalized to 1 which gives the angular distribution of mosaic blocks. N is the number of unit cells per cm^3, $F^{\pm} = 4(b \pm p)$ is the structure factor, θ_β is the Bragg angle and t is the average path length in the crystal.

All the experiments were performed by symmetric transmission of a crystal of uniform thickness. For this case, the secondary extinction problem can be solved exactly and the reflectivity function is given by [23]

$$g = 1/2\,(1 - e^{-2g_o})\, e^{-\mu t} \qquad (2\text{-}17)$$

where g is the crystal reflectivity with extinction and where μ is the linear absorption coefficient. This gives for the measured flipping ratio

$$R_{ext.} = \frac{1 - e^{-2g_o^{+}}}{1 - e^{-2g_o^{-}}} \qquad (2\text{-}18)$$

In order to evaluate (2-16) some assumptions must be made to make the integral tractable. Assume the neutron path length t is constant over the crystal, which amounts to neglecting edge effects, and assume $W(\theta_\beta - \phi)$ is Gaussian so that the mosaic block distribution is given by

$$W(\theta_\beta - \phi) = \frac{1}{\sqrt{2\pi}\ \eta}\ e^{\frac{-(\theta_\beta - \phi)^2}{2\eta^2}} \qquad (2\text{-}19)$$

The integral in (2-16) over $d\theta$ will depend on the angular and wavelength divergence of the incident beam as well as the mosaic block spread. Some assumption must thus be made as to the relative importance of the mosaic distribution and the beam spread in angle and wavelength in producing broadening of the Bragg peak. Q is much more slowly varying in λ than the beam distribution and can be taken outside the integral in (2-16).

If we assume that the broadening resulting from the mosaic distribution of the crystal is much smaller than that from beam divergence effects, the integral in (2-16) becomes

$$\int W(\theta_\beta - \phi)\, d\phi = \frac{1}{\sqrt{2\pi}\ \eta} \int_{-\infty}^{+\infty} e^{-(\theta_\beta - \phi)^2/2\eta^2}\, d(\theta_\beta - \phi) = \frac{1}{2\sqrt{\pi}\ \eta} \qquad (2\text{-}20)$$

then

$$R_{ext.} = \frac{1 - \exp\frac{-Q^+ t}{\sqrt{\pi}\ \eta}}{1 - \exp\frac{-Q^- t}{\sqrt{\pi}\ \eta}} = \frac{Q^+}{Q^-}\ \frac{\left[1 - \frac{Q^+ t}{2\sqrt{\pi}\ \eta}\right]}{\left[1 - \frac{Q^- t}{2\sqrt{\pi}\ \eta}\right]} \qquad (2\text{-}21)$$

assuming that $\frac{1}{2\sqrt{\pi}\ \eta}\ Q^{\pm} t << 1$ which is always true in the cases in which we are interested.

If we assume that the broadening due to the beam divergence is much smaller than that caused by the mosaic spread but larger than that of a perfect mosaic block, we immediately obtain, using (2-16), (2-18), and (2-19),

$$R_{ext.} = \frac{Q^+}{Q^-} \quad \frac{\left[1 - \frac{Q^+ t}{\sqrt{2\pi}\ \eta}\right]}{\left[1 - \frac{Q^- t}{\sqrt{2\pi}\ \eta}\right]} \qquad (2\text{-}22)$$

The actual case is somewhere between the results given by (2-21) and (2-22). In the crystals used for the reflections where extinction is largest, the broadening due to the mosaic width was larger than the broadening due to beam spread, so we will adopt equation (2-22). We will see later in this section that an absolute value of the term multiplying Q^{+}_{-} is not generally needed to make the extinction correction, so the actual form taken is not important. Thus, making use of the fact that

$$R = \left(\frac{1 + p/b}{1 - p/b}\right)^2 = \frac{Q^+}{Q^-} \qquad (2\text{-}23)$$

and using (2-22) we obtain

$$R_{ext.} = R \left[1 - \frac{Q^+ t}{\sqrt{2\pi}\ \eta} \left(1 - \frac{1}{R_{ext.}}\right)\right] . \qquad (2\text{-}24)$$

Then

$$\frac{\Delta R}{R} = \frac{R - R_{ext.}}{R} = \frac{Q^+ t}{\sqrt{2\pi}\ \eta} \quad \frac{4\ p/b}{(1+p/b)^2} \qquad (2\text{-}25)$$

and

$$\Delta p/b = \frac{Q^+ t}{\sqrt{2\pi}\ \eta}\ p/b \left(\frac{1 - p/b}{1 + p/b}\right) \qquad (2\text{-}26)$$

where $\Delta p/b$ is the error introduced by neglecting extinction entirely. The data can then be corrected for secondary extinction by the expression

$$p/b = \frac{\sqrt{R_{ext.}} - 1}{\sqrt{R_{ext.} + 1}} + \Delta p/b \quad . \tag{2-27}$$

In order to make the extinction correction, $\frac{Q^+ t}{\sqrt{2\pi}\ \eta}$ must be known.

This term will be used often, so let us denote it by the letter A. The extinction correction is always small, so the measured value of the magnetic scattering amplitude can be used in finding Q^+. Some knowledge of the Debye-Waller factor is also needed to find Q^+, but this knowledge can be very approximate as the correction is not particularly sensitive to the Debye-Waller factor. The Debye-Waller factor was calculated by using a characteristic temperature of $400^{\circ}K$ given by James [24] for nickel. Everything is then known in the term A except for the factor η which is a measure of the angular distribution of the mosaic blocks in the sample. In theory, η is simply related to the width at half maximum of the sample rocking curve taken with a sharp monochromating crystal in such a geometry that the rocking curve width is minimized. The relation is $\eta = \frac{\beta}{2.36}$ where β is the rocking curve width at half maximum. It is found in practice that the rocking curves show a very irregular mosaic distribution, and it is usually difficult, if not impossible, to get a value of η that is satisfactory for the entire crystal sample. The beam size can be reduced so as to look at only a small portion of the sample, and in this case, the rocking curve becomes more regular as only a small part of the total mosaic distribution is examined. Even in this case, however, the parameter η deduced from the rocking curve must be treated as quite unreliable. Rocking curves for the

A-2-1 sample are shown in Fig. 2.

A better approach to finding the correction term A for various crystals is to minimize the extinction in one case to such an extent that $R_{ext.} = R$ for a given reflection, preferably the first reflection. Once the correct value of R is obtained for a given sample, the A value of other sample crystals can be found using the relationship

$$A = \frac{R - R_{ext.}}{R - 1} \quad . \tag{2-28}$$

The extinction can be made small by decreasing the crystal thickness. For the (111) reflection, crystal slices as thin as 0.0038 cm. were used for long counting periods in an effort to find R. Measurements from a set of crystal slices of various thicknesses can be used to get the correct value of R by extrapolating to zero sample thickness. The preparation and cutting of the crystals is discussed in Appendix B.

If the flipping ratio is measured at different wavelengths for a given crystal, R can be eliminated between two equations like (2-23) and the value of A for the crystal can be obtained. Measurements were made on several crystals for the (111) reflection at wavelengths of 1.05 $\mathring{A}$ and 0.77 $\mathring{A}$. The crystals can also be examined at different reflections and values of A obtained through the angular dependence of the extinction correction. By a series of intercomparisons, a reliable value of the extinction correction factor A can be found for each sample crystal. In some cases, the sample rocking curves were uniform enough to give a reasonable estimate of the parameter η. The values of A determined from these values of η were in good agreement with the values of A determined using (2-23). In no case, however, was any reliance placed on the value of A determined from a crystal slice rocking curve. A table of the

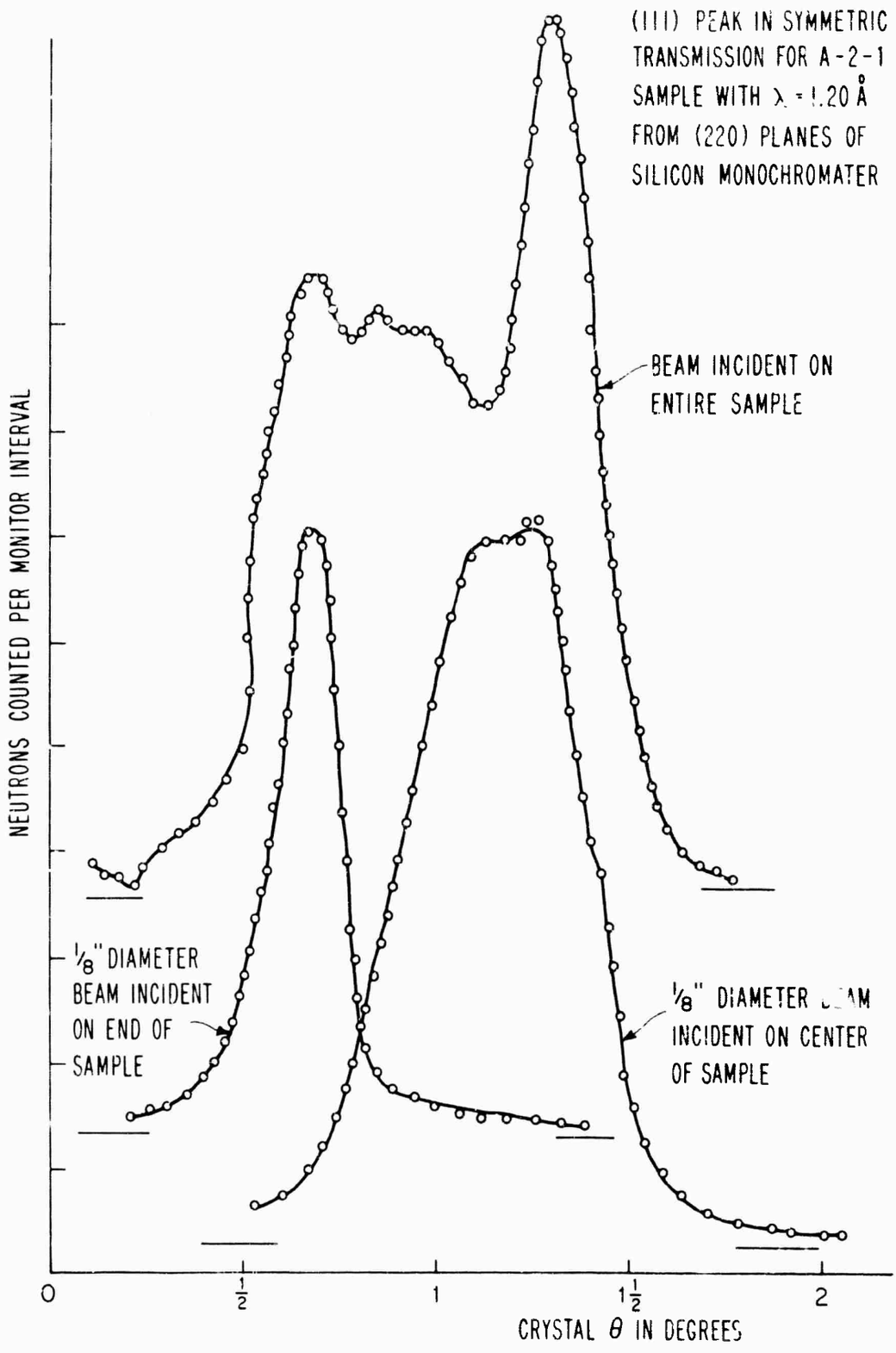

FIG. 2 TYPICAL CRYSTAL ROCKING CURVES

BLANK PAGE

A values of some of the sample crystal slices is given below for $\lambda = 1.05\ A^{o}$.

TABLE I

Secondary Extinction Correction Factors for Various Samples

Sample	Reflection	Sample Thickness in Cm.	A
A-2-1	(111)	0.056	$0.314 \pm .008$
A-3-1	(111)	0.021	$0.077 \pm .007$
A-4	(111)	0.010	$0.056 \pm .006$
A-2-2	(111)	0.0038	$0.000 \pm .008$
B-3-b	(200)	0.023	$0.171 \pm .007$

2. Primary Extinction

Primary extinction results from the reduction in neutron intensity seen by those atoms at the bottom of a mosaic block relative to those at the top of the block where the neutron beam enters. There are several expressions available for correcting for primary extinction in the X-ray case. The well-known Darwin Theory for primary extinction can be carried over to the neutron case by replacing Zachariasen's [25] factor A_p for X-rays by

$$A_p = \frac{\lambda t_o F^{\pm} N}{\cos \theta_\beta} \tag{2-29}$$

where t_o is the thickness of a mosaic sheet. In this case, the flipping ratio is given by

$$R = R_{ext.}^{pri.} \frac{A_p + \sum_{n=o}^{\infty} J_{2n+1}(2A_p^{-})}{A_p - \sum_{n=o}^{\infty} J_{2n+1}(2A_p^{+})} \tag{2-30}$$

where J_n is a Bessel function of order n. Since $A_p^{\pm}$ is small, the Bessel function can be expanded in the usual manner giving

$$R = R_{ext.}^{pri.} \left[1 + 1/12 \frac{\lambda^2 t_o^2 N^2}{\cos^2 \theta_\beta} (F^{+2} - F^{-2}) \right] . \qquad (2\text{-}31)$$

The Darwin formulation is derived for a thin plate of infinite lateral extent. It would seem more reasonable to consider a formulation for a small perfect spherical crystalline, and correction expressions taking this point of view are available from Ekstein [26]. Using the Ekstein formulation, one obtains in a similar manner

$$R = R_{ext.}^{pri.} [1 + 7/16 \, N^2 \lambda^2 t_o^2 (F^{+2} - F^{-2})] . \qquad (2\text{-}32)$$

For secondary extinction, the correction to the flipping ratio can be written using (2-22)

$$R = R_{ext.}^{sec.} \left[1 + \frac{\lambda^3 T_o N^2}{\sqrt{2\pi} \sin 2\theta_\beta \cos \theta_\beta} (F^{+2} - F^{-2}) \right] \qquad (2\text{-}33)$$

T_o being the sample thickness. We see that the expressions for correcting for primary and secondary extinction are very similar. Unfortunately, there is no way to measure accurately the thickness t_o of a mosaic block, so we have no idea as to the exact size of the primary extinction correction. For any reasonable estimate of the thickness of a mosaic block, however, the correction term is very small.

Combining both primary and secondary extinction corrections and keeping only first-order terms, the flipping ratio becomes

$$R = R_{ext.} \left[1 + \lambda^2 N^2 (F^{+2} - F^{-2}) \left(7/16\, t_o^2 + \frac{\lambda T_o}{\sqrt{2\pi} \sin 2\theta_\beta \cos\theta_\beta} \right) \right] \quad (2-34)$$

Notice that the primary extinction term containing t_o has a different dependence on θ_β than the secondary extinction term containing T_o. We can thus hope to be able to sort out the relative importance of the correction terms by considering reflections at different Bragg angles. Equation (2-34) can be rewritten as

$$\left[\frac{R}{R_{ext.}} - 1 \right] \frac{\sin 2\theta_\beta \cos\theta_\beta}{F^{+2} - F^{-2}} = 7/16\, \lambda^2 N^2 t_o^2 \sin^2\theta_\beta \cos\theta_\beta + \frac{\lambda^2 N^2 T_o}{\sqrt{2\pi}\,\eta} = \xi \ . \quad (2-35)$$

R, and thus $F^{\pm}$, can be obtained by using a very thin bent crystal slice which would have small primary and secondary extinction. The correction formula can then be tried out on a thick crystal slice which has large secondary extinction and presumably larger primary extinction than a thin bent slice. If we compute ξ and examine its angular dependence we can decide which correction terms are important. If all the extinction in the thick slice is secondary extinction ξ should be independent of the Bragg angle. If there is appreciable primary extinction, ξ should be some function of the Bragg angle. ξ is plotted in Fig. 3 as a function of the Bragg angle for the A-2-1 slice which is .022 inch thick and has 25% secondary extinction at the (111) reflection. We see that ξ is independent of angle within the experimental error. Unfortunately, in the Ekstein case the difference in angular dependence of the primary and secondary extinction correction terms is small. We can probably say from Fig. 3, however, that primary extinction in the A-2-1 slice does not cause more than a 1% error in the flipping ratio.

BLANK PAGE

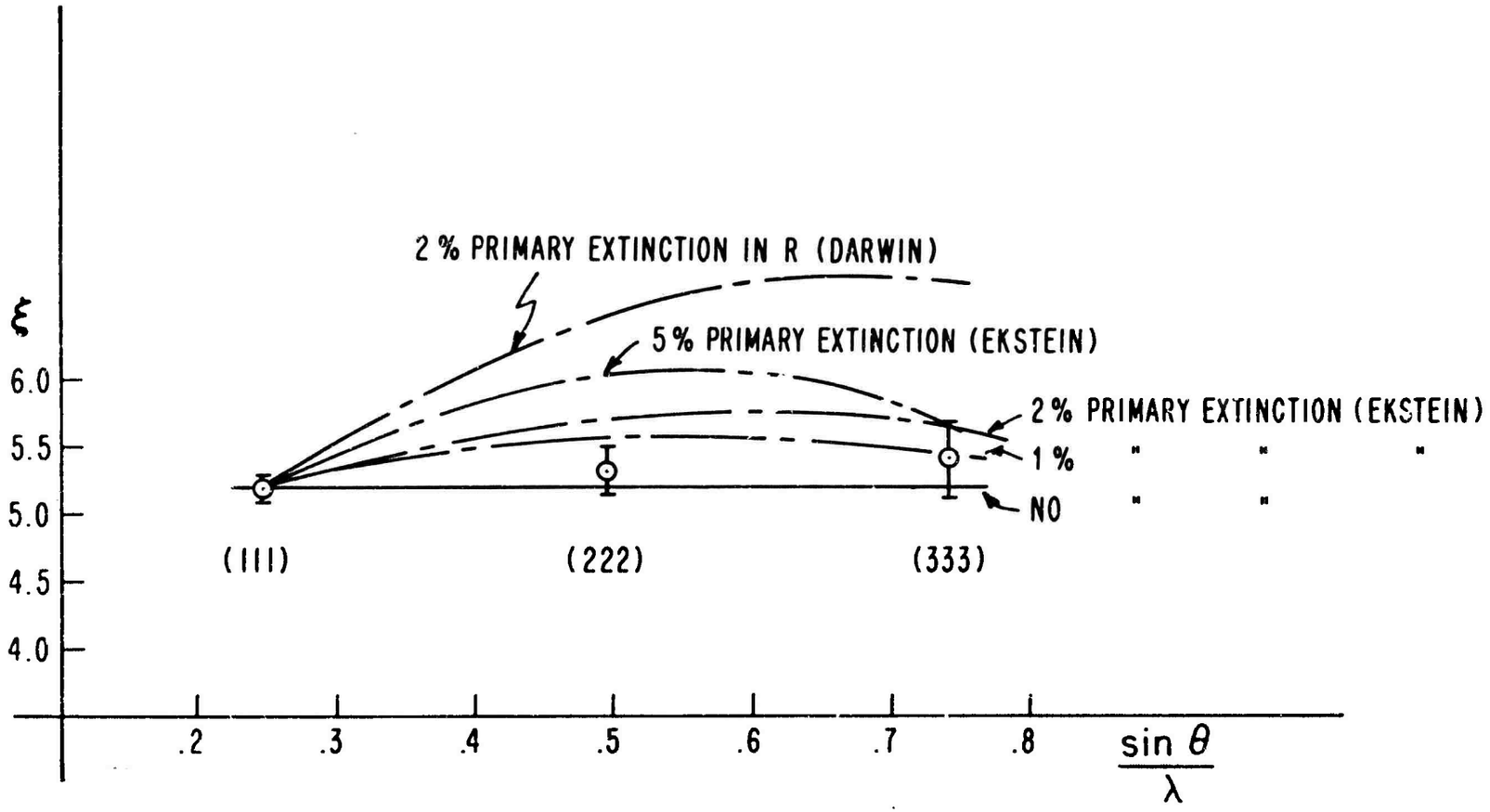

FIG. 3 PRIMARY EXTINCTION CORRECTION

This gives a sufficiently small error in p/b that the error caused by primary extinction can be neglected in comparison with other experimental errors. Therefore, in all cases we have assumed that any contributions from primary extinction to the data are negligible and have only corrected for secondary extinction effects.

C. Multiple Reflections

In finding the magnetic scattering amplitude by the flipping ratio measurement, it is assumed that the neutron scatters just once from the planes corresponding to the Bragg peak being measured. There are certain orientations of the sample crystal that permit reflections, in addition to the Bragg reflection, that one wishes to observe. Moon and Shull [27] have shown that these simultaneous reflections have a large effect on the neutron intensity diffracted by single crystals. The effect of simultaneous reflections will tend to cancel somewhat in the flipping ratio; nevertheless, the effects are still large enough that they must be correctly taken into account particularly for the first few reflections. For this reason, all the data were taken while the sample was rotated slowly around the scattering vector $\bar{K}$. Any abrupt changes in the Bragg reflected intensity as the sample is rotated about $\bar{K}$ are an indication of multiple reflections and the data in that region were disregarded. Multiple reflections usually are more prominent when there is appreciable secondary extinction, and little multiple scattering was observed in the thin crystal slices used for most of the measurements. Figure 4 shows data taken for the thick A-2-1 slice and the thin A-4 slice as they were rotated about $\bar{K}$ for the (222) reflection. The sizeable intensity changes with rotational angle for the A-2-1 slice are the result of multiple reflections. The effect is particularly noticeable when the

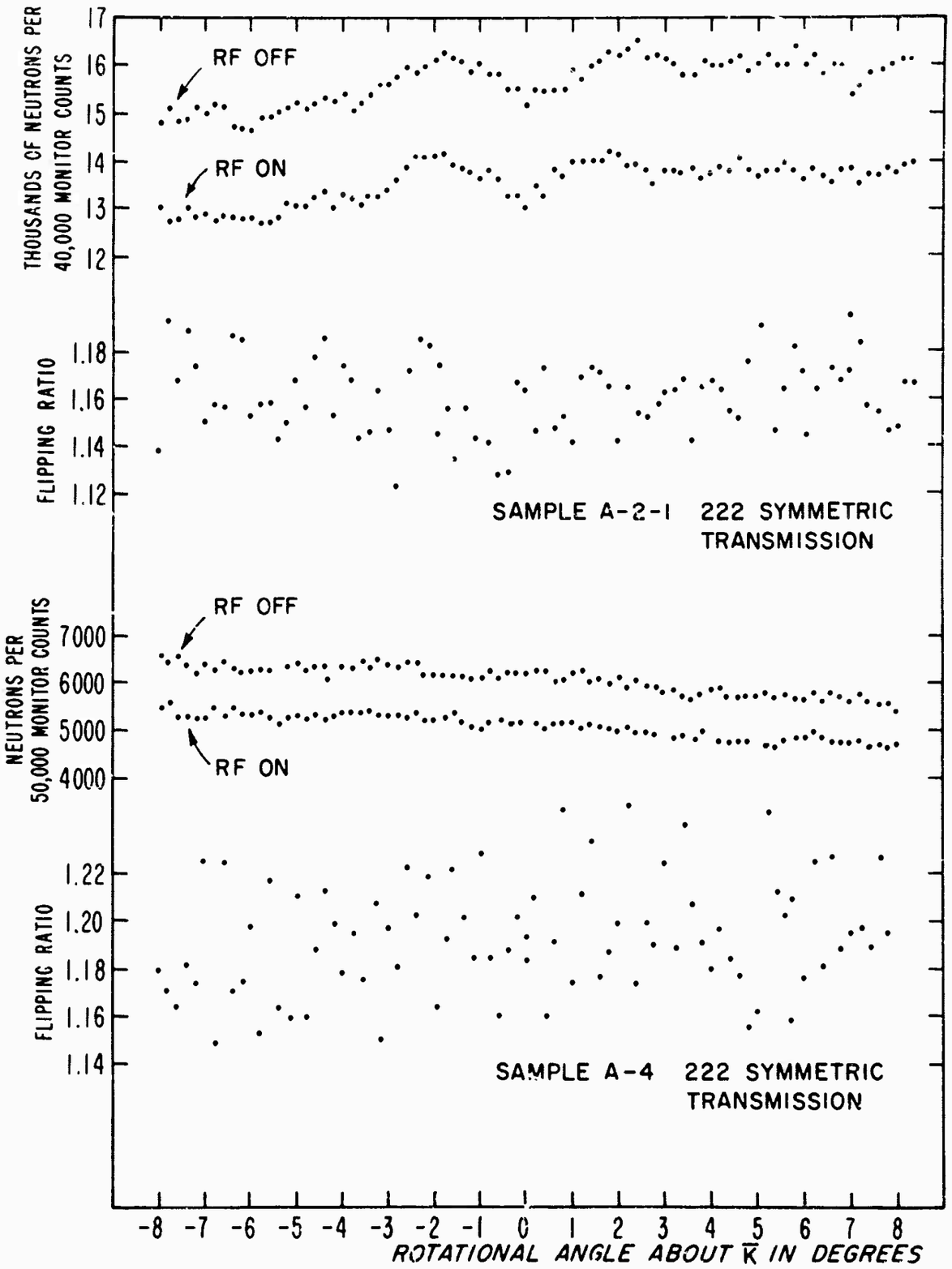

FIG. 4 MULTIPLE REFLECTION EFFECTS

rotational angle is zero and the crystal slice is perpendicular to the neutron beam. The A-4 crystal slice intensities show no multiple scattering effects.

D. Sample Depolarization

We have so far assumed that the sample is magnetically saturated perpendicular to the plane of scattering defined by the incoming and outgoing neutron beam. The flipping ratio of the (220) reflection was looked at as a function of the applied magnetic field. Figure 5 shows that R did not vary with field in the region of ~ 7000 oe. used throughout the experiment, and it can be assumed that the sample was completely saturated in this region. A very sensitive check on the extent of saturation of the sample crystal can be made by examining the beam depolarization caused by the crystal [28]. This can be accomplished by using two $Co_{.92}\ Fe_{.08}$ polarizing crystals and examining the change in the flipping ratio when the sample is placed between them, but still in the 7000 oe. field. The experimental arrangement is shown in Fig. 6. The beam depolarization was measured for each sample and found to be very small in each case verifying that the sample was very close to complete saturation.

So far, it has been assumed that the sample crystal slice was straight up and down in the magnetic field. The data, however, were taken with the sample being rotated around the vector $\bar{K}$ in order to correct for multiple reflections. The neutron spin precesses about the direction of the total magnetic field given by

$$\bar{B} = \bar{H} + (4\pi - N)\,\bar{M} \qquad (2\text{-}36)$$

where N is a demagnetizing factor. Because of the $(4\pi - N)\,\bar{M}$ term, the direction of $\bar{B}$ in a tilted sample will be different from the incident neutron polarization direction, and this will cause depolarization of the neutron beam in the sample.

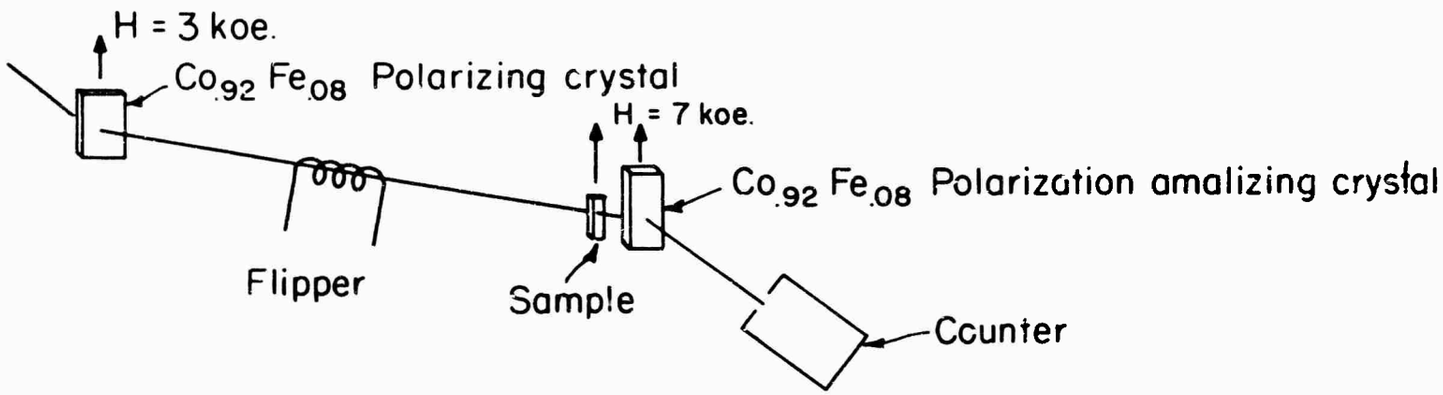

FIG. 5 EXPERIMENTAL ARRANGEMENT FOR MEASURING SAMPLE DEPOLARIZATION

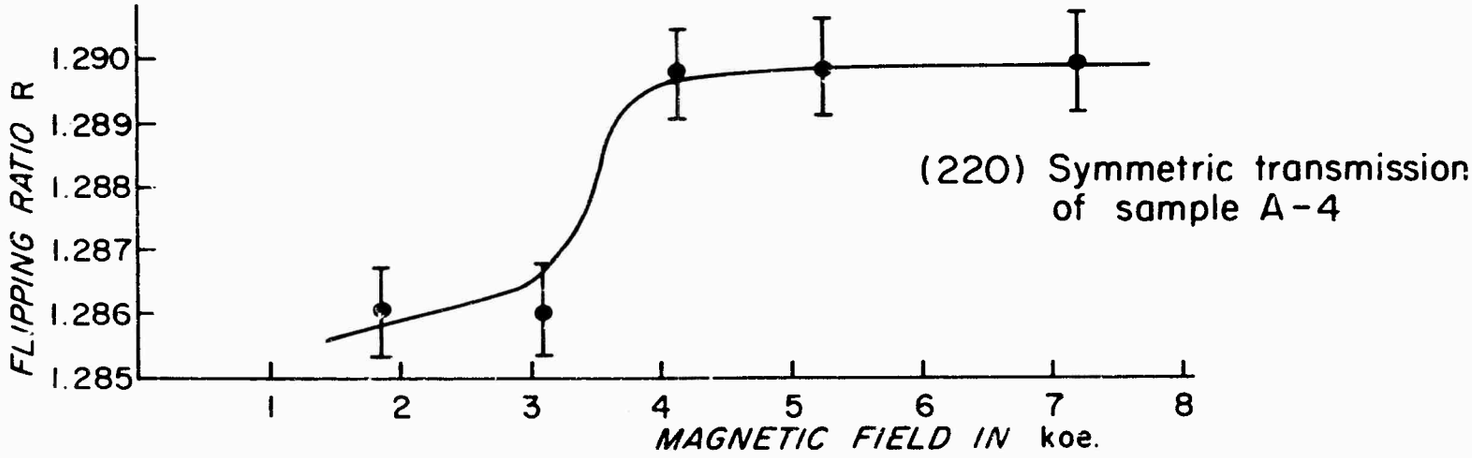

FIG. 6 FLIPPING RATIO VERSUS APPLIED MAGNETIC FIELD

Halpern and Holstein [28] have shown that this problem can be treated classically, and Moon [11] has treated the case where $\bar{M}$ is not along $\bar{H}$ in the sample crystal due to magnetic anisotropy but with the sample slice straight up and down in the applied magnetic field. Moon's treatment also assumed the sample slice was many neutron Larmor precessions long.

The neutron polarization direction is always along $\bar{B}$, and the magnitude of the polarization inside the sample is given by

$$P = P_o \cos\gamma \qquad (2\text{-}37)$$

where γ is the angle between $\bar{B}$ inside the sample and $\bar{B}$ outside the sample. This is the so-called sudden approximation and in our case amounts to assuming that the fields at the sample edge change rapidly over a Larmor precession length. An attempt was made to measure the depolarization of a crystal slice tilted in a magnetic field using the same arrangement as Fig. 6 but including a provision for changing the tilting or azimuthal angle of the slice. It is found that the neutron precession time in fields that we are concerned with is such that the neutron makes only a few precessions in traversing the sample crystal slice. The neutron polarization on leaving the slice will then depend on the extent to which an integral number of precessions is completed in the slice. If the neutron spin makes an integral number of precessions in the sample, it rotates back to its original direction on leaving the slice and no depolarization is observed. If, on the other hand, the neutron makes a half integral number of precessions, the polarization on leaving the sample is less than the polarization inside the sample and is given by

$$P = P_o \cos 2\gamma \qquad (2\text{-}38)$$

Intermediate cases can also be calculated and the general case is given in Appendix C. The observed depolarization of the tilted crystal slice depends on its tilting angle, its thickness, its shape (through its demagnetizing factors) and its

saturation magnetization. Figure 7 shows the result of a depolarization experiment for the sample A-4 which is slightly over a Larmor precession length thick. The theoretical curve comes from the deviation in Appendix C. From the results, it is found that if the tilting angle is limited to 10^{o}, negligible error is introduced in the measured values of p/b. If larger tipping angles are desired, depolarization corrections could be applied using the methods of Chapter II, Section A.

E. Temperature Dependent Effects

All measurements were made at room temperature. In this case, a thermal average of the ratio of magnetic to nuclear scattering is being measured. This can be written

$$< p/b >_T = p/b < M_z > e^{+[W_n(K^2) - W_e(K^2)]} \qquad (2\text{-}39)$$

where $< M_z >$ is the time average of the z component of the unit magnetic moment vector. The exponential term consists of the difference between the Debye-Waller factors for nuclear scattering and magnetic electron scattering. As mentioned in Chapter I, Section B, it is assumed that the nuclei and their electrons move together in such a way that their Debye-Waller factors are the same and the exponent in (2-34) vanishes. The only temperature effect would then be the variation of $< M_z >$ with temperature, and this would be proportional to the variation in the saturation magnetization per unit mass with temperature. Following Bozorth [29], the magnetization at room temperature for nickel is taken to be .946 of that at zero degrees Kelvin.

There have been several temperature dependent flipping ratio measurements made and no evidence has been found that p/b is strongly temperature dependent except for the expected change in magnetization. Pickart and Nathans [12] checked

BLANK PAGE

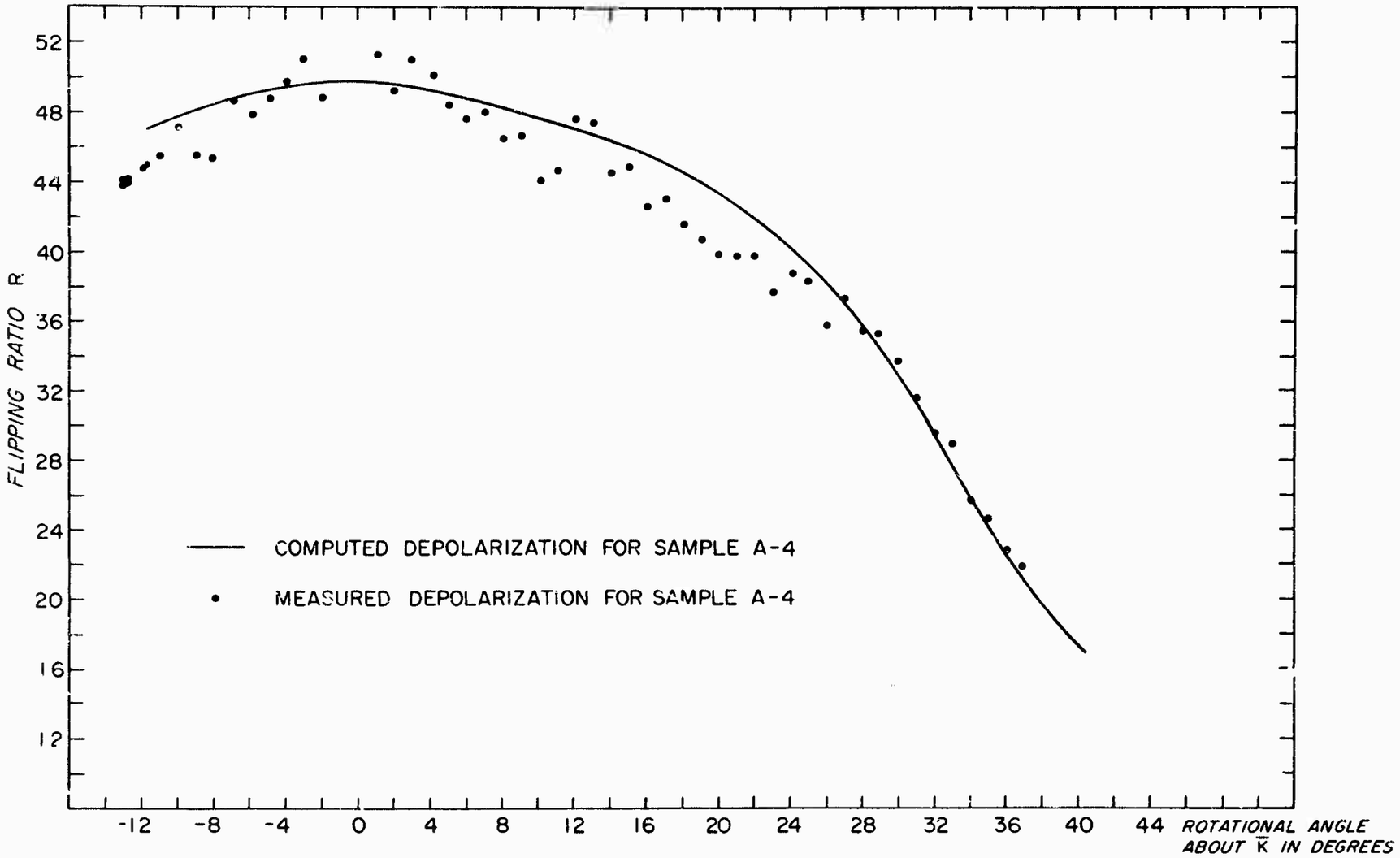

FIG. 7 SAMPLE DEPOLARIZATION EFFECTS

several reflections in Fe_3Al at 77°K and found no variation in p/b from that at room temperature outside of the change in magnetization. Shull [10] measured two iron reflections particularly sensitive to the e_g to t_{2g} ratio and found no temperature dependence in the asymmetry of the spin distribution in the temperature region between 78° and 830°K. Moon [11] examined three cobalt reflections at 78°K and found no temperature dependence in p/b except for the magnetization change. Menzinger and Paoletti [30] have found a small temperature dependence in p/b in f.c.c. cobalt at 873°K that cannot be explained by the change in magnetization. This may stem from a temperature dependence in the magnetic form factor or a difference in the Debye-Waller factors for nuclear and magnetic scattering at high temperatures.

Considering the above results, it would seem reasonable to assume that p/b in nickel is only temperature dependent through its magnetization through most of the temperature range from 0°K to the Curie temperature. The temperature dependence of p/b may not follow the magnetization in the temperature range near the Curie point, but Shull's results on iron suggest that the asymmetry in the magnetic moment distribution is probably temperature independent.

Saenz [31] has shown that the inelastic scattering of neutrons by spin waves peaks rather sharply around the Bragg reflections in a ferromagnet. If this scattering is of substantial intensity, it could cause an error in the background correction to the flipping ratio. For the magnetic field geometry employed, the cross section for spin wave scattering is minimized and is polarization independent. The effect of spin wave inelastic scattering was assumed negligible at room temperature and no correction was made for it.

III. DISCUSSION OF RESULTS

A. General Remarks

The magnetic scattering amplitude was measured for the first 27 Bragg reflections. About nine months of neutron counting time was required since the magnetic scattering is small in nickel. A summary of the measured data is given in Appendix D.

There are two approaches that can be taken in analyzing the scattering data. The first is to compare the results with calculated values. The comparison has to be made with Hartree-Fock free atom calculations since no wavefunction calculations are available for nickel atoms contained in a metal lattice. We will see that free atom calculations fit the data very closely if a constant negative term is added to the magnetization. The second approach is to Fourier-transform the measured data to obtain the periodic magnetic moment distribution directly. This method does not require advance knowledge of the 3d wavefunctions and gives a three-dimensional map of the periodic magnetic moment density independent of any model of the magnetization.

The magnetic scattering amplitude for the (000) reflection cannot be measured but can be calculated from the magnetization. If we take the magnetization of nickel to be $0.606\,\mu_\beta$ per atom [32] at zero degrees K and the relative magnetization at room temperature to be 0.946 of that at zero degrees K [29], the magnetic scattering amplitude for the (000) reflection at room temperature is given by

$$p(000) = \frac{\gamma e^2}{mc^2} \frac{\langle n_\beta \rangle}{2} = 0.1545 \times 10^{-12} \text{cm}. \qquad (3\text{-}1)$$

where n_β is the room temperature number of Bohr magnetons per atom and γ is the neutron gyromagnetic ratio.

To find the magnetic scattering amplitude from the measured data we must know the nuclear scattering amplitude. $1.03 \pm .01 \times 10^{-12}$ cm. is the accepted value of the nuclear scattering amplitude in nickel [21]. The form factor is given by the magnetic scattering amplitude normalized to unity at (000) and is given in Table 2. A 1% error in the normalization of the form factor has been included to take account of the uncertainty in our knowledge of the nuclear scattering amplitude. The form factor is consistently higher than that measured by Nathans et al. [9]. This difference probably results from their improperly accounting for secondary extinction. All of the data of Nathans et al. were taken on a relatively thick 0.022" crystal slice whose mosaic character was assumed to require no correction for secondary extinction.

The periodic magnetic moment density is given by a superposition of the moment distributions centered at each lattice site i,

$$\rho(r) = \sum_i \rho(\bar{r}-\bar{r}_i) = \frac{n_\beta}{(2\pi)^3} \sum_i \int dK\, e^{-i\bar{K}\cdot(\bar{r}-\bar{r}_i)} f(K) =$$

$$\frac{n_\beta}{V} \sum_\tau e^{-2\pi i \bar{\tau}\cdot\bar{r}} f(\tau) \qquad (3\text{-}2)$$

where τ is a reciprocal lattice vector, V the unit cell volume, and $\rho(r)$ is measured in Bohr magnetons per cubic Angstrom. We see that only the values of the form factor determined at the Bragg reflections are needed to obtain the periodic magnetic moment density. However, $\rho(r)$, cannot give us any information about parts of the moment distribution that are not periodic. For instance, a measurement of the magnetic scattering at the Bragg reflections cannot give any information about magnetic clusters. Letting p (h k ℓ) be the magnetic scattering amplitude, equation (3-2) can be written

TABLE II

Comparison of Calculated and Measured Form Factors

h k ℓ	sin ϑ/λ	f(K)		$\langle j_o \rangle$	$\langle j_4 \rangle$	orbit	core	f(K)cal	Δ
(111)	0.246	0.791	±0.009	0.654	0.014	0.755	0.005	0.784	-0.002
(200)	0.284	0.701	±0.008	0.578	0.020	0.700	0.006	0.687	-0.014
(220)	0.401	0.446	±0.005	0.357	0.045	0.520	0.007	0.446	0.000
(311)	0.472	0.320	±0.005	0.271	0.060	0.430	0.007	0.318	-0.002
(222)	0.493	0.310	±0.004	0.237	0.072	0.405	0.007	0.323	0.013
(400)	0.569	0.156	±0.003	0.154	0.075	0.325	0.005	0.157	0.001
(331)	0.618	0.168	±0.003	0.116	0.081	0.281	0.005	0.170	0.002
(420)	0.636	0.131	±0.003	0.105	0.083	0.266	0.004	0.130	-0.001
(422)	0.696	0.107	±0.004	0.066	0.088	0.220	0.002	0.105	-0.002
(511)	0.739	0.036	±0.004	0.055	0.091	0.192	0.002	0.043	0.007
(333)	0.739	0.109	±0.003	0.055	0.091	0.192	0.002	0.111	0.002
(440)	0.804	0.058	±0.004	0.033	0.092	0.155	0.000	0.063	0.005
(531)	0.841	0.032	±0.004	0.022	0.091	0.138	0.000	0.039	0.007
(600)	0.853	-0.025	±0.003	0.019	0.091	0.135	-0.001	-0.019	0.006
(442)	0.853	0.052	±0.004	0.019	0.091	0.135	-0.001	0.056	0.004
(620)	0.899	-0.009	±0.004	0.004	0.089	0.117	-0.002	-0.014	-0.006
(533)	0.932	0.036	±0.004	0.000	0.089	0.105	-0.002	0.031	-0.005
(622)	0.943	0.005	±0.004	0.000	0.088	0.103	-0.002	-0.002	-0.007
(444)	0.984	0.037	±0.004	-0.006	0.087	0.090	-0.003	0.033	-0.004
(551)	1.015	0.009	±0.004	-0.008	0.085	0.085	-0.003	0.009	0.000
(711)	1.015	-0.047	±0.004	-0.008	0.085	0.085	-0.003	-0.044	0.003
(640)	1.025	-0.001	±0.004	-0.011	0.084	0.080	-0.003	-0.004	-0.003
(642)	1.063	+0.001	±0.004	-0.013	0.082	0.070	-0.002	0.001	0.000
(713)	1.091	-0.026	±0.004	-0.017	0.081	0.065	-0.002	-0.027	-0.001
(553)	1.091	0.012	±0.004	-0.017	0.081	0.065	-0.002	0.011	-0.001
(800)	1.137	-0.063	±0.004	-0.019	0.077	0.055	-0.002	-0.062	0.001
(733)	1.164	-0.017	±0.004	-0.022	0.074	0.050	-0.002	-0.018	-0.001

$$\rho(r) = \frac{1}{V}\left[n_\beta n + \frac{2mc^2}{\gamma e^2}\sum_{hk\ell}\left(\sum_j p(hk\ell)e^{i\bar{K}\cdot\bar{r}_j}\right)e^{-i\bar{K}\cdot\bar{r}}\right] \qquad (3\text{-}3)$$

where the summation j extends over all the atoms of the unit cell and n is the number of atoms in the unit cell. The sum over h k ℓ is to be taken over all h k ℓ both positive and negative but should not include the term (000). The neutron measurements determine the magnetic scattering amplitudes p (h k ℓ) in magnitude and sign and thus give the shape of $\rho(r)$ in absolute terms, but say nothing about the normalization of ρ (. We can rewrite (3-2) as

$$\rho(r) = \overline{\rho} + \rho'(r) \qquad (3\text{-}4)$$

where $\overline{\rho}$ and $\rho'(r)$ correspond respectively to the first and higher terms in equation (3-2). If $\rho'(r)$ integrated over r contains a different magnetic moment than is obtained in the magnetization measurement, the zero level determined by $\overline{\rho}$ must be shifted so the integral of $\rho(r)$ over r gives the correct total moment. Consider the case where we have two crystals in which $\rho'(r)$ is the same but with different magnetization values. The neutron diffraction measurements would give the same values for p(h k ℓ) but the normalized form factors would have a different shape. We thus see that the proper way to compare form factors is to test their proportionality at all h k ℓ values other than (000); i.e., two form factors correspond to equal radial distributions when $f_1(K) = C\, f_2(K)$, $K \neq 0$. It is important to remember this when comparing measured form factors with calculated form factors.

B. Comparison of the Data with Calculated Results

In the derivation for magnetic scattering in Chapter I, we assumed the orbital moment was quenched and included only the spin part of the form factor. This would be the case if g=2.00 where g is the spectroscopic splitting factor The deviation of g from 2.00 gives a measure of the orbital contribution to

the total magnetic moment. Specifically, $\frac{g-2}{g}$ is the fraction of the total magnetic moment which is due to orbital motion. For nickel, g= 2.20 as given by the magnetomechanical measurements of Scott [33]; so almost 10% of the magnetic moment is due to orbital motion. An orbital contribution must thus be included in our form factor expression and the spin contribution reduced by 2/g.

There is also some scattering from the core electrons inside the 3d shell. The core contains as many electrons with spin up as with spin down, but the radial distribution of spin up and spin down electrons is slightly different [20] due to exchange effects. This difference in radial distributions results in a small amount of scattering from the core and we will include a core polarization term in our form factor expression.

The measured form factor $f(\bar{K})$ may thus be written as the sum of three contributions

$$f(\bar{K}) = \frac{2}{g} f_{spin}(\bar{K}) + \frac{g-2}{g} f_{orbit}(\bar{K}) + f_{core}(\bar{K}) \qquad (3-5)$$

where $f_{spin}(\bar{K})$ is a normalized spin density form factor, $f_{orbit}(\bar{K})$ is a normalized orbital form factor, and $f_{core}(\bar{K})$ is a normalized core polarization form factor.

Since 3d free atom form factors are available, we would like to compare our measured form factor with them. As we have seen, this is properly done by seeing if the free atom form factor can be scaled to agree with the measured form factor at all reflections other than (000). We wish, however, to deal with normalized form factors and we will assume the form factor can be written

$$f(\bar{K}) = (1+\alpha)\, f_{3d}(\bar{K}) - \alpha\, \delta(\bar{K}) \qquad (3\text{-}6)$$

where α is a constant; $\alpha\delta(\bar{K})$ makes a contribution at K=0 only, and thus corresponds to a uniform contribution to the magnetization. By using expression (3-6) we can compare the radial distribution of spin density in nickel metal with that in a free atom and still deal with normalized form factors.

The measured form factor in nickel is not a smooth function of $\frac{\sin\theta}{\lambda}$. Notice, for instance, that the (422) and (600) reflections fall at the same value of $\frac{\sin\theta}{\lambda}$ but have very different scattering amplitudes. This means that the spin density must be different along different directions in the crystal lattice. In a cubic field, the five-fold degenerate orbitals of the 3d electrons split into triply degenerate t_{2g} orbitals which transform like xy, xz, and yz, and doubly degenerate e_g orbitals which transform like $3z^3 - r^2$ and $x^2 - y^2$. The neutron scattering amplitudes from these two sets of orbitals are different, and Weiss and Freeman [34] have shown that the spin form factor for 3d electrons in a cubic field can be written

$$f_{3d}(\bar{K}) = \langle j_o \rangle + (5/2\ \gamma - 1)\, A_{hk\ell}\, \langle j_4 \rangle \qquad (3\text{-}7)$$

where $\langle j_o \rangle$ represents the spherical part of the spin distribution and $\langle j_4 \rangle$ the aspherical part. γ is the percentage of 3d electrons in e_g orbitals and is equal to 40% for spherical symmetry.

$A_{hk\ell}$ is a function of the direction that is being examined in the crystal and is given by

$$A_{hk\ell} = \frac{h^4+k^4+\ell^4-3(h^2k^2+h^2\ell^2+k^2\ell^2)}{(h^2+k^2+\ell^2)^2} \qquad (3\text{-}8)$$

The $\langle j_n \rangle$ represent various moments of the radial spin density $\rho(r)$ and are given by

$$\langle j_n \rangle = \int \rho(r)\, J_n(Kr)\, dr \qquad (3\text{-}9)$$

where $J_n(Kr)$ is spherical Bessel function of order n.

Blume [4] has derived an expression for the orbital form factor, and using his notation it is given by

$$f(K)_{\text{orbit}} = (g_o - 1/2\, g_2) + (5/2\, \gamma\text{-}1)\, A_{hkl}\, (3/14\, g_4 - 1/2\, g_2) \qquad (3\text{-}10)$$

where the first term gives the spherical contribution and the second term gives the aspherical contribution. One finds that $(3/14\, g_4 - 1/2\, g_2)$ is much smaller than $\langle j_4 \rangle$ and we will leave it out of our form factor expressions. Using equations (3-4), (3-6), (3-7), and (3-10) the form factor expression becomes

$$f(\bar{K}) = 2/g\, (1+\alpha)\, [\, \langle j_o \rangle + (5/2\, \gamma\text{-}1)\, A_{hkl} \langle j_4 \rangle\,] + \frac{g-2}{g} [g_o - 1/2\, g_2]$$

$$+ f_{core}\, (\bar{K}) + 2/g\, \alpha \delta\, (\bar{K}) \qquad (3\text{-}11)$$

Hartree Fock calculations of $\langle j_o \rangle$ have been performed by Freeman and Watson for nickel in various stages of ionization [20], [35], [36]. $\langle j_o \rangle$ is given for Ni, Ni^+, Ni^{++} and Ni^{+++} taking all the outer electrons to be in the 3d shell. and for the free atom $3d^8\, 4s^2$ configuration [35]. The $\langle j_o \rangle$'s for Ni, Ni^+, Ni^{++} and Ni^{+++} are plotted in Fig. 8. It is found that the $\langle j_o \rangle$ for the $3d^8 4s^2$ configuration is very similar to that for Ni^{++} so it is not plotted separately. $\langle j_o \rangle$ has also been calculated for Ni^{++} using an unrestricted Hartree-Fock technique that allows wavefunctions with differing spin quantum numbers m_s to have different radial functions [20]. The form factor is determined from a density that involves the difference of the two radial func-

BLANK PAGE

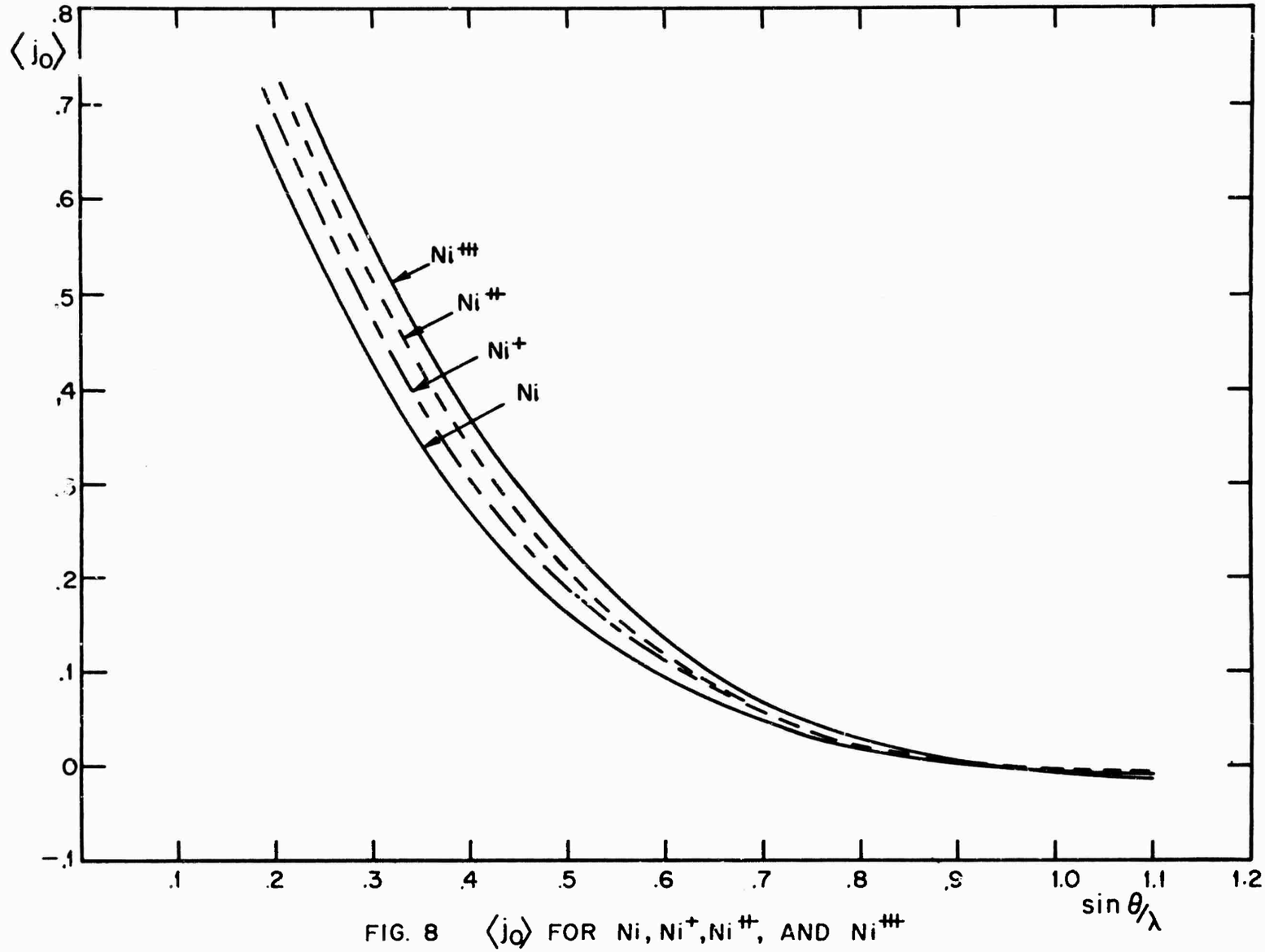

FIG. 8 $\langle j_0 \rangle$ FOR Ni, Ni^{+}, Ni^{++}, AND Ni^{+++}

tions for the two spin states and is slightly expanded relative to the form factor given by the restricted Hartree-Fock calculation. The $\langle j_o \rangle$ from an unrestricted Hartree-Fock calculation for Ni^{++} in a cubic field arising from an octahedral array of point charges is also available [34]. The $\langle j_o \rangle$'s for the three Ni^{++} calculations is shown in Fig. 9.

Hartree-Fock free atom calculations for $\langle j_4 \rangle$ have been performed for Ni, Ni^{+}, Ni^{++}, and Ni^{+++} [35]. $\langle j_4 \rangle$ is plotted in Fig. 10 for each of the above cases. The orbital contribution $(g_o - 1/2 g_2)$ was obtained from A. J Freeman [37]. It is similar to a spin form factor being only slightly more expanded in $\frac{\sin \theta}{\lambda}$. The orbital form factor is given in Table II.

The data were compared with all these calculations and the best fit was obtained using the $\langle j_o \rangle$ from the unrestricted Hartree-Fock calculation for Ni^{++}, the $\langle j_4 \rangle$ for Ni^{++} and setting $\gamma = 19\%$ and $\alpha = 0.19$. The comparison of the measured and calculated form factors is shown in Fig. 11.

The agreement is extraordinarily good. $f(\bar{K})$ is very sensitive to the calculation chosen for $\langle j_o \rangle$ and it is easy to determine which calculation is best. The form factor is not very sensitive to the calculation taken for $\langle j_4 \rangle$ and either Ni^{+}, Ni^{++}, or Ni^{+++} will give a good fit with $\gamma = 19\%$. $\langle j_o \rangle$ is not needed to find γ since $\langle j_o \rangle$ can be eliminated between two equations like (3-11) written for the same value of $\frac{\sin \theta}{\lambda}$ but for different values of h k ℓ. It is best to do this at $\frac{\sin \theta}{\lambda}$ values ranging from 0.8 to 1 Å^{-1} where $\langle j_4 \rangle$ is large and fairly constant. In practice, the best way to determine γ is to Fourier-transform differences between calculated and measured results for various values of γ. For the correct value of

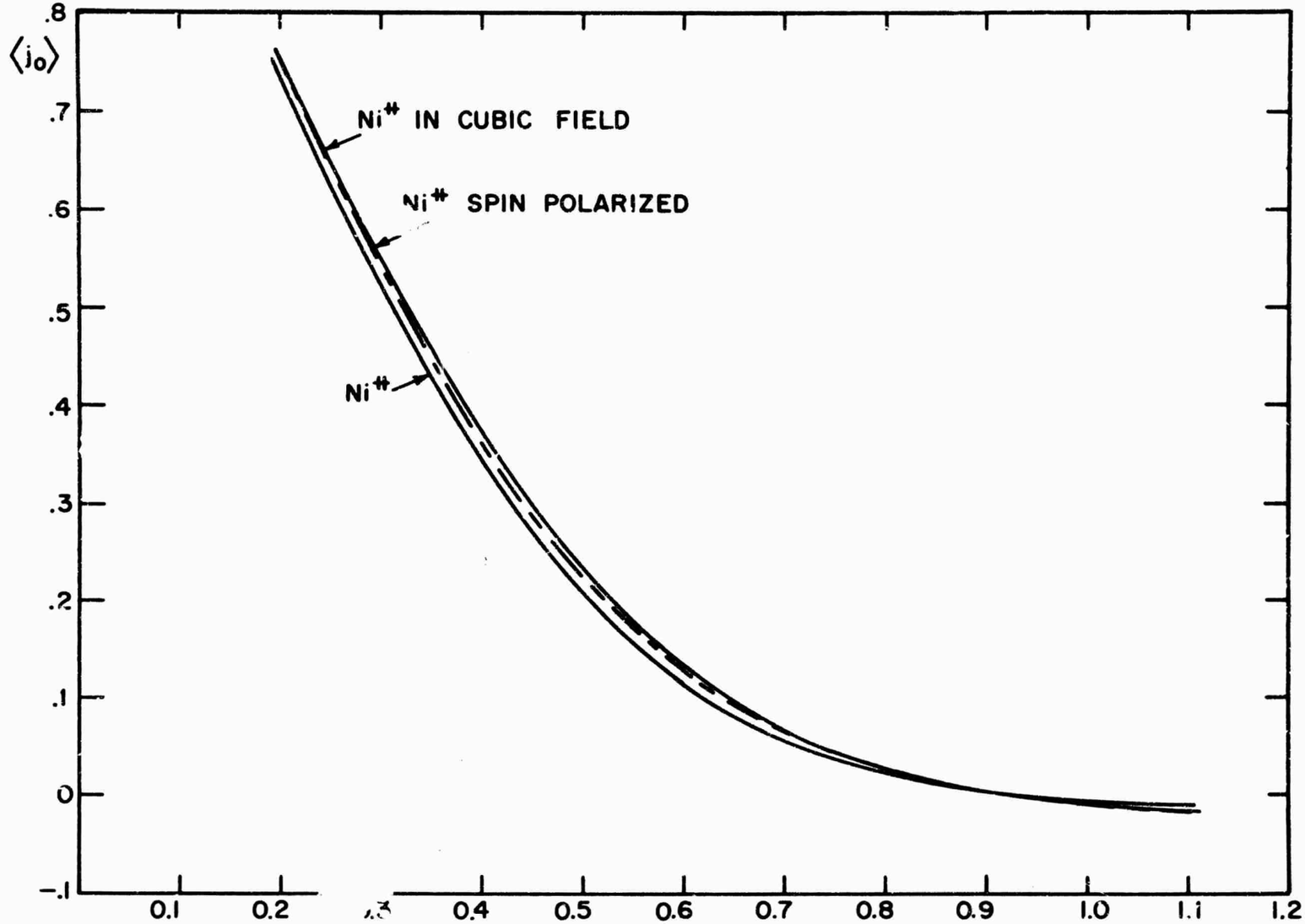

FIG. 9 ⟨j_0⟩ FOR VARIOUS HARTREE FOCK CALCULATIONS ON Ni^{++}

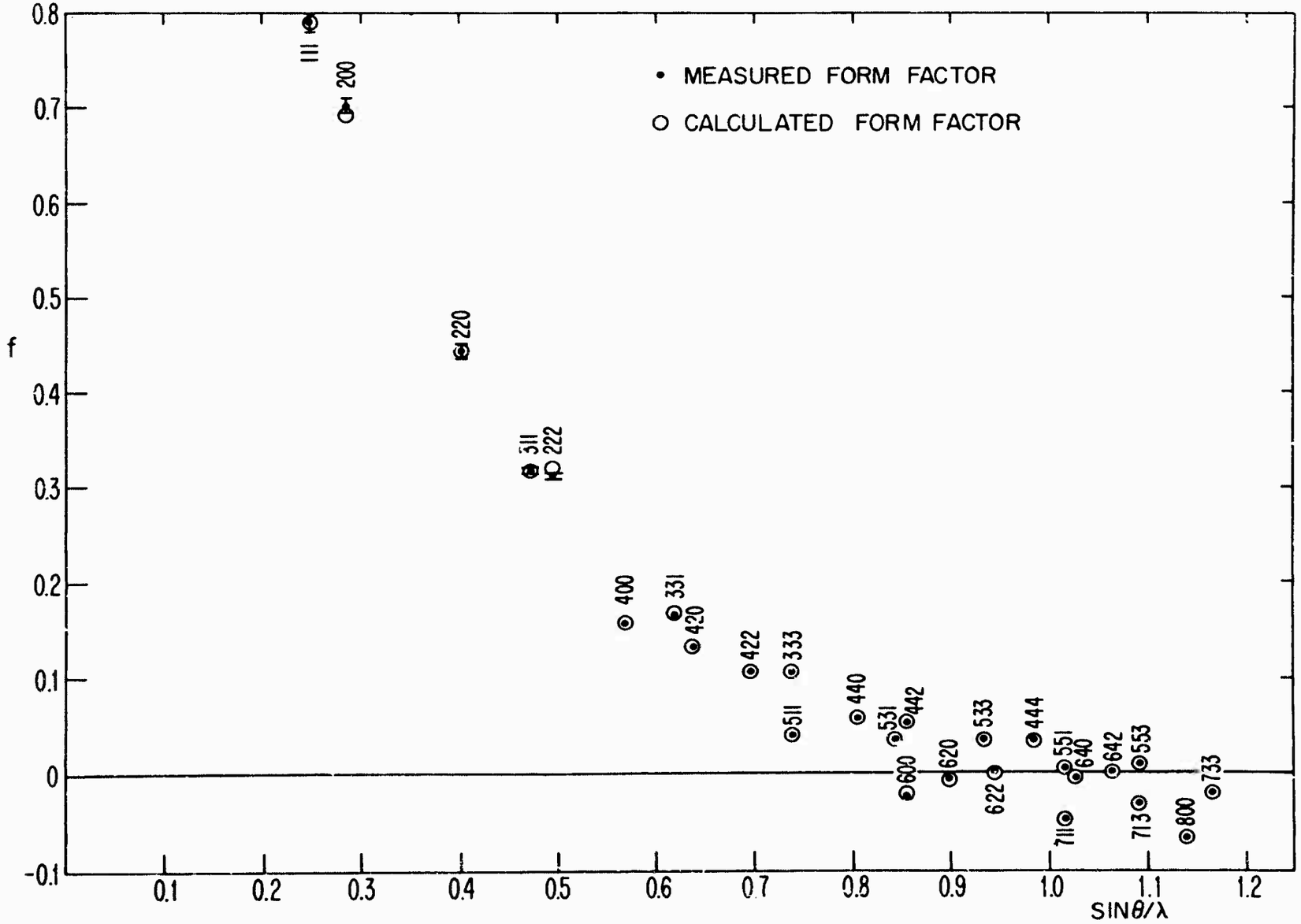

FIG. II COMPARISON OF CALCULATED AND MEASURED FORM FACTORS

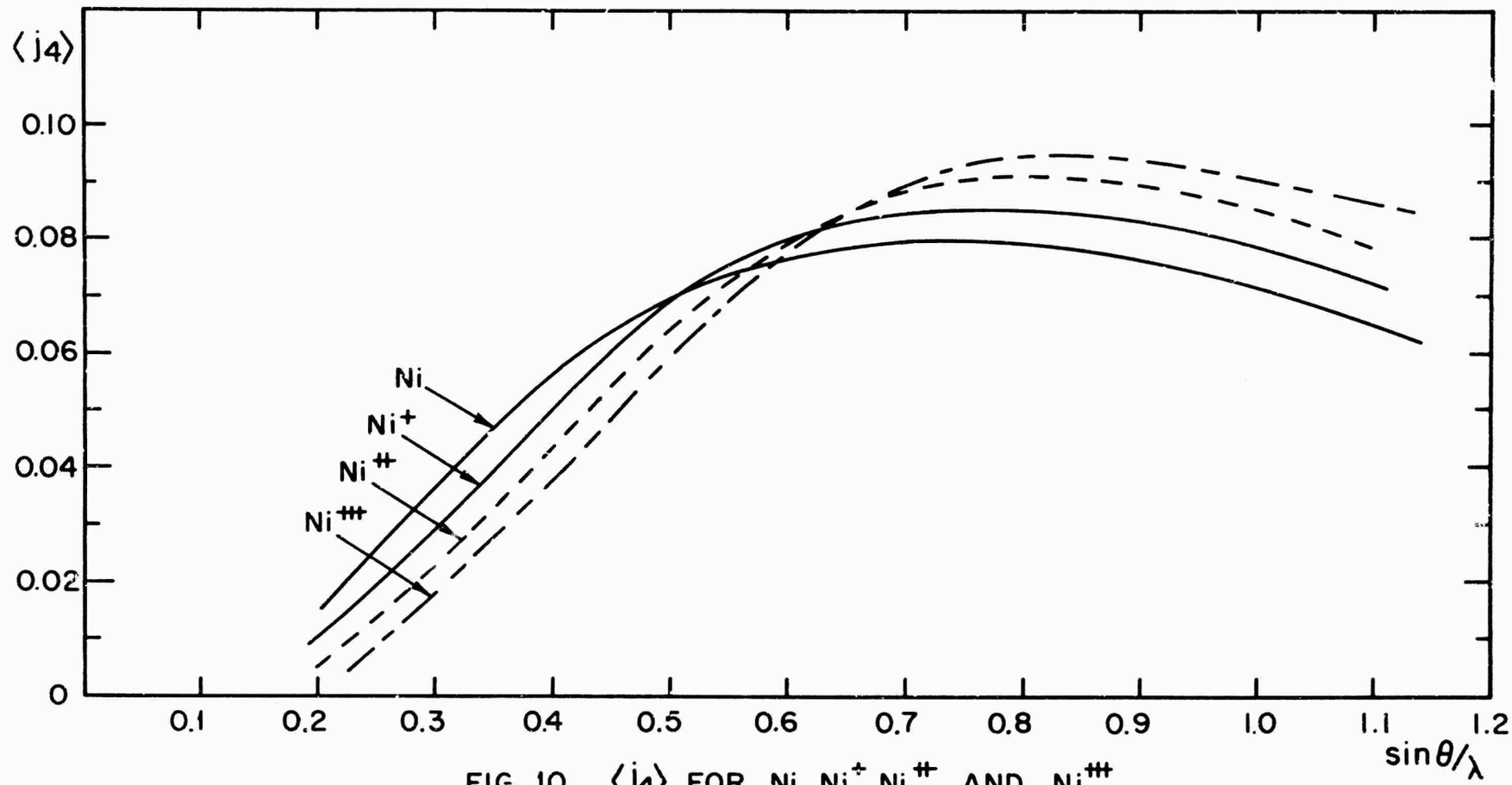

FIG. 10 $\langle j_4 \rangle$ FOR Ni, Ni^{+}, Ni^{++}, AND Ni^{+++}

BLANK PAGE

Y the Fourier transform of the difference will have spherical sy. metry. In this manner, it was determined that $19 \pm 1\%$ of the 3d magnetic electrons are in the e_g orbitals.

Figure 11 shows that the shape of the spin distribution in metallic nickel is almost identical to the shape of the free atom spin distribution. We have obtained this agreement by scaling the 3d free ion form factor by 19%, and thus in order to obtain the correct value for the magnetization we must include a constant negative contribution to the spin density. Since we cannot see the point K = 0 by neutron diffraction techniques, none of our measurements is of any assistance in determining the origin of the negative constant density. One possibility is that the negative constant represents 4s electrons oppositely polarized to the 3d electrons. 4s electron form factors fall to immeasurably small values before the first Bragg reflection and thus can be represented by a delta function as in (3-10). There would also be 3d, 4s cross terms in the form factor from the admixing of the 3d, 4s wavefunctions. It is difficult to determine the exact nature of this 3d, 4s cross term. It is expected that it should be very small. Certainly, the cross term would have a $\bar{K}$ dependence unlike either the 3d or the 4s form factor, and the good agreement between the measured and the free atom form factor would be ruined by such a term if it were at all sizable. We are probably safe in assuming the cross term can be neglected in comparison with the other contributions to the form factor.

In this case, since the neutrons scatter from an unpaired spin density, either 3d or 4s, (3-11) can be taken to represent a form factor which includes both 3d and 4s electrons. The neutron data are thus in agreement with a model of the spin density which distributes the net magnetic moment per atom at $0^{\circ}K$.

in the following way;

$$3d\ \text{Spin} = +0.656\ \mu_\beta$$

$$4s\ \text{Spin} = -0.105\ \mu_\beta$$

$$3d\ \text{Orbit} = +0.055\ \mu_\beta$$

If the 4s spin density were spread uniformly throughout the unit cell, it would amount to a constant magnetization field of $-.0097\ \mu_\beta/\text{A}^{\circ\,3}$ or 1.2 kg.

It is also plausible that the parameter α represents scattering from parts of the 3d band that have wavefunctions very unlike free atom wavefunctions. As mentioned in Chapter I, the wavefunctions at the top of the 3d band are very similar to 3d free atom wavefunctions, and this is presumably why the 3d free atom form factor provides the good fit to the data shown in Fig. 10.

The 3d wavefunctions at the bottom of the band are quite diffuse. There is no net difference in the number of electrons with spin up and spin down at the bottom of the band. However, scattering can still take place from the bottom of the band if there is a difference in the radial distribution of spin up and spin down electrons. Watson and Freeman's unrestricted Hartree-Fock calculation on Ni^{++} shows that there is some variation in the radial wavefunctions for spin up and spin down electrons in the free atom. Freeman [37] has suggested that, in a metal, these spin polarization effects can act like an effective negative moment in the region far removed from the lattice sites and may be sufficient to account for the value of α. In other words, if the exact 3d wavefunctions including spin polarization effects could be obtained for the metal, a form factor calculated from these wavefunctions would fit the data without the necessity of scaling it. Along these lines, L. Hodges, N. D. Lang, and H. Ehrenreich [38] appear to be having some

success in calculating a 3d form factor for nickel metal using a pseudopotential method in a band calculation. Although only preliminary results are available, it appears that it may not be necessary to include negative 4s electron polarization to obtain a fit between the measured form factor and the form factor derived from the band calculations.

If one believes that all the scattering results from the 3d band, the asymmetry function $\langle j_4 \rangle$ should be calculated from a ρ (r) that applies to the scaled 3d free atom form factor, and not just the 3d free atom form factor itself. A function $\langle j_4 \rangle$ which corresponds to the $\rho(r)$ actually measured was supplied by R. J. Weiss [39] and is plotted in Fig. 12. This function is not very different from the $\langle j_4 \rangle$ for $Ni^{\#}$, and since the form factor is not very sensitive to the exact shape of $\langle j_4 \rangle$ it is impossible to say if the Weiss $\langle j_4 \rangle$ gives a better fit to the data than the $\langle j_4 \rangle$ for the $Ni^{\#}$ free ion. Using the Weiss $\langle j_4 \rangle$, the best fit is obtained with an e_g population of 20% which is a very small change from the 19% required with the free ion calculation. An e_g population of $19 \pm 1\%$ seems to be valid regardless of the origin of the constant.

It is worthwhile noting that scaling the free atom 3d form factors also gives a very good fit to the measured form factors in both iron and cobalt [10-11]. The value of α is 0.10 for iron and 0.18 for cobalt. It seems that any theory that ascribes the origin of α to the 3d band must also have to be valid in iron and cobalt.

It is conceivable that expression (3-1) for p (000) is incorrect in a metal and that no scaling factor is actually needed. This seems very unlikely as there is no experimental evidence that (3-1) is incorrect. The magnetic cross section expressions from which (3-1) is derived give the correct ex-

BLANK PAGE

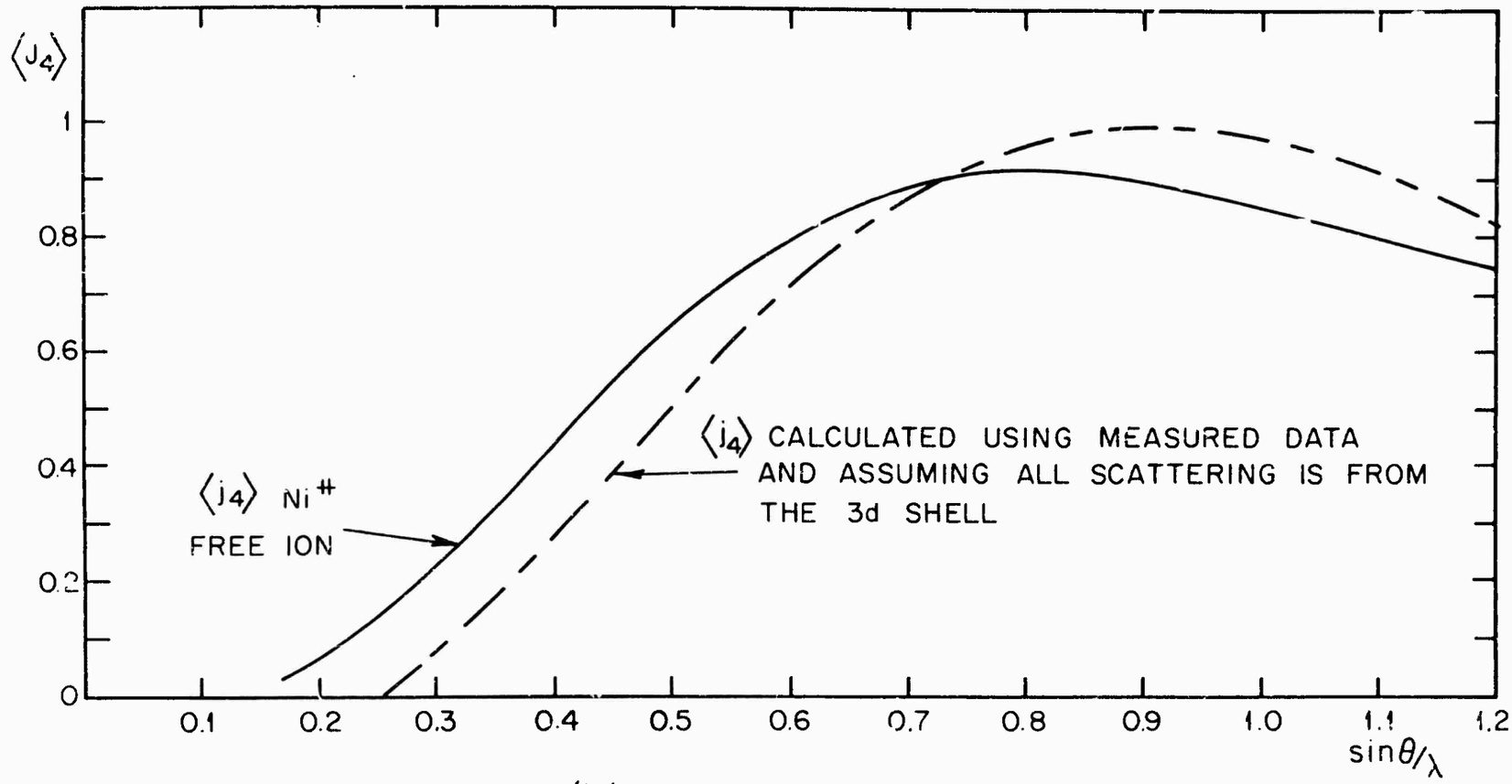

FIG. 12 COMPARISON OF $\langle j_4 \rangle$ DERIVED FROM MEASURED DATA WITH FREE ATOM HARTREE FOCK CALCULATION FOR $\langle j_4 \rangle$

perimental results for the magnetic scattering in salts, and for paramagnetic scattering. Moreover, if the magnetic amplitude expression (3-1) were incorrect, we should expect to have found a common scaling factor α for the three cases, iron, cobalt, and nickel, whereas these are not the same. In any case, since the scaled free atom form factors fit the neutron diffraction data so extraordinarily well for iron, cobalt, and nickel, it seems that free atom-like wavefunctions must play a very fundamental role in describing the periodic spin density in these metals.

C. Fourier Inversion

In Section B we have seen that the measured data are in good agreement with a model of the magnetic moment density that superimposes free atom-like distributions on a constant negative background. By using equation (3-3), the Fourier summation can be performed to give the magnetic moment distribution directly from the measured data and the calculated point at (000). It would be interesting to see how the distribution given by the Fourier inversion compares with the model used in Section B.

The three-dimensional summation was done on the M.I.T. Computation Center 7094 computer using the MIFRI Fourier Summation Program [40]. Figure 13 shows the magnetic moment density along the three main crystallographic directions. As we expect, since the 3d electrons in nickel have 81% t_{2g} symmetry, the magnetic moment density $\rho(r)$ is spread out along the [111] direction relative to the [100] direction. The density $\rho(r)$ falls to zero quite rapidly and the magnetic moment density over most of the unit cell is very small.

The density $\rho(r)$ shown in Fig. 13 is really the true density as seen with finite resolution, since data are only available up to the (733) reflection at

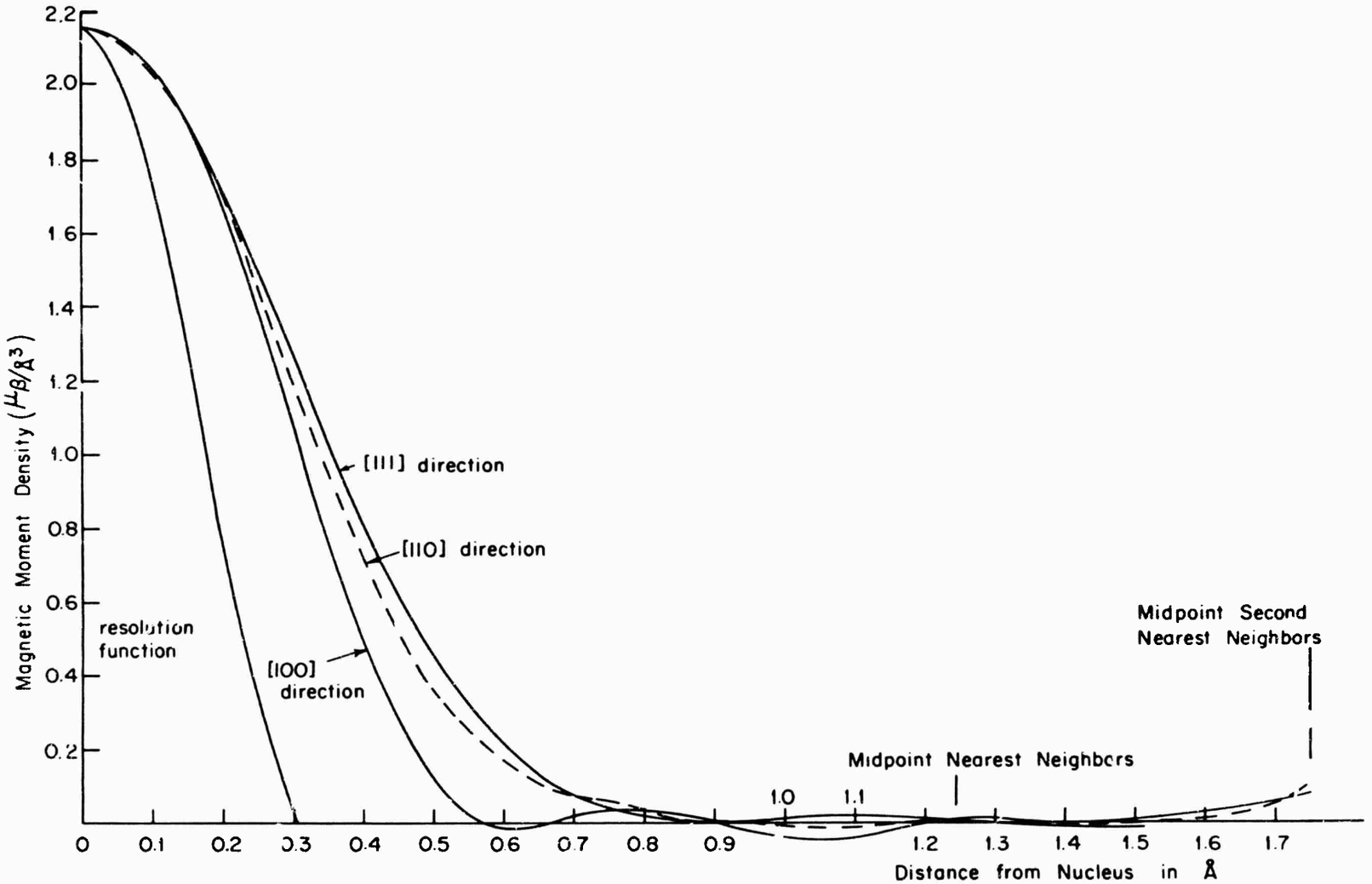

FIG. 13 DISTRIBUTION OF MAGNETIC MOMENT DENSITY ALONG THE THREE MAJOR CRYSTALOGRAPHIC DIRECTIONS.

BLANK PAGE

$\sin\frac{\theta}{\lambda} = 1.16\ \text{Å}^{-1}$. This is the optical equivalent of viewing an object through a finite-sized aperture. The resolution function in Fig. 13 is obtained by Fourier-transforming a constant form factor for all reflections up to and including (733), and letting the form factor be zero for all higher reflections. The resolution function shows the diffraction effects that would be produced in attempting to map a lattice of points using the same set of reflections used in the nickel measurements. Any detail finer than the width at half maximum of the resolution function cannot be resolved. We know, for instance, that the magnetic moment density from the 3d shell should be zero at the atomic site. The diffraction broadening effect of limited data smears out the moment density so that the decrease in the 3d moment near the atomic site is not observed.

The limited resolution also causes the $\rho(r)$ obtained from the Fourier series to oscillate at large r. We would like to be able to determine the size of the moment density in the region between atoms, but the oscillations obscure the real value of $\rho(r)$ which is smaller than the amplitude of the oscillations. The problem is that the Fourier series for $\rho(r)$ converges too slowly to give us the information we are asking for, namely, the moment density in the region between the atoms. This problem has been solved by deriving the Fourier series that gives $\rho(r)$ averaged in space over a small cubic block. The Fourier series for the average $\overline{\rho}(r)$ is given by

$$\overline{\rho(r)} = \frac{n_\beta}{V} \int_{x-\delta}^{x+\delta} \int_{y-\delta}^{y+\delta} \int_{z-\delta}^{z+\delta} \sum_{hk\ell} F_{hk\ell} e^{-2\pi i (h x/a + k y/a + \ell z/a)} d_x d_y d_z$$

$$= \frac{n_\beta}{V} \frac{1}{(2\pi \delta/a)^3} \sum_{hk\ell} \frac{F_{hk\ell}}{hk\ell} \sin(2\pi h \delta/a) \sin(2\pi k \delta/a) \sin(2\pi \ell \delta/a)$$

$$\times e^{-2\pi i (h x/a + k y/a + \ell z/a)} \qquad (3\text{-}12)$$

where $F_{hk\ell}$ is the magnetic structure factor, a the lattice constant, and δ/a is 1/2 of the length of a side of the cubic block over which the average is taken. This series converges much more rapidly than the series given in (3-2) because of the factor $(hk\ell)^{-1}$. The convergence of the two series for the point (1/2 00) is shown in Fig. 14 for $\delta/a = .075$. The continued sum of the Fourier series is plotted versus $\frac{\sin\theta}{\lambda}$, so successive points are obtained by increasing the number of terms in the series by one, except the average is shown when two reflections fall at the same $\frac{\sin\theta}{\lambda}$ value. The size of the oscillations is a measure of the convergence of the series.

The $\rho(r)$ determined by (3-3) is still oscillating widely at $\frac{\sin\theta}{\lambda}_{o\,3} = 1.16$, but the series for $\overline{\rho(r)}$ has converged nicely to the value $-0.0085\ \mu_\beta / A$. Several different cube sizes $(2\delta/a)^3$ were tried. Good convergence has been obtained with blocks as small as 0.07 lattice constants on each side. For much smaller blocks $\overline{\rho(r)}$ does not converge well and would approach the $\rho(r)$ given by (3-3) if the cube became small enough. If the block is large, the moment in the region of the atom is smeared out over the entire cell. For intermediate sizes of δ/a the Fourier series for $\overline{\rho}(r)$ converges to a negative density of $0.0085\ \mu_\beta / A^3$ uniformly over the entire unit cell outside of the

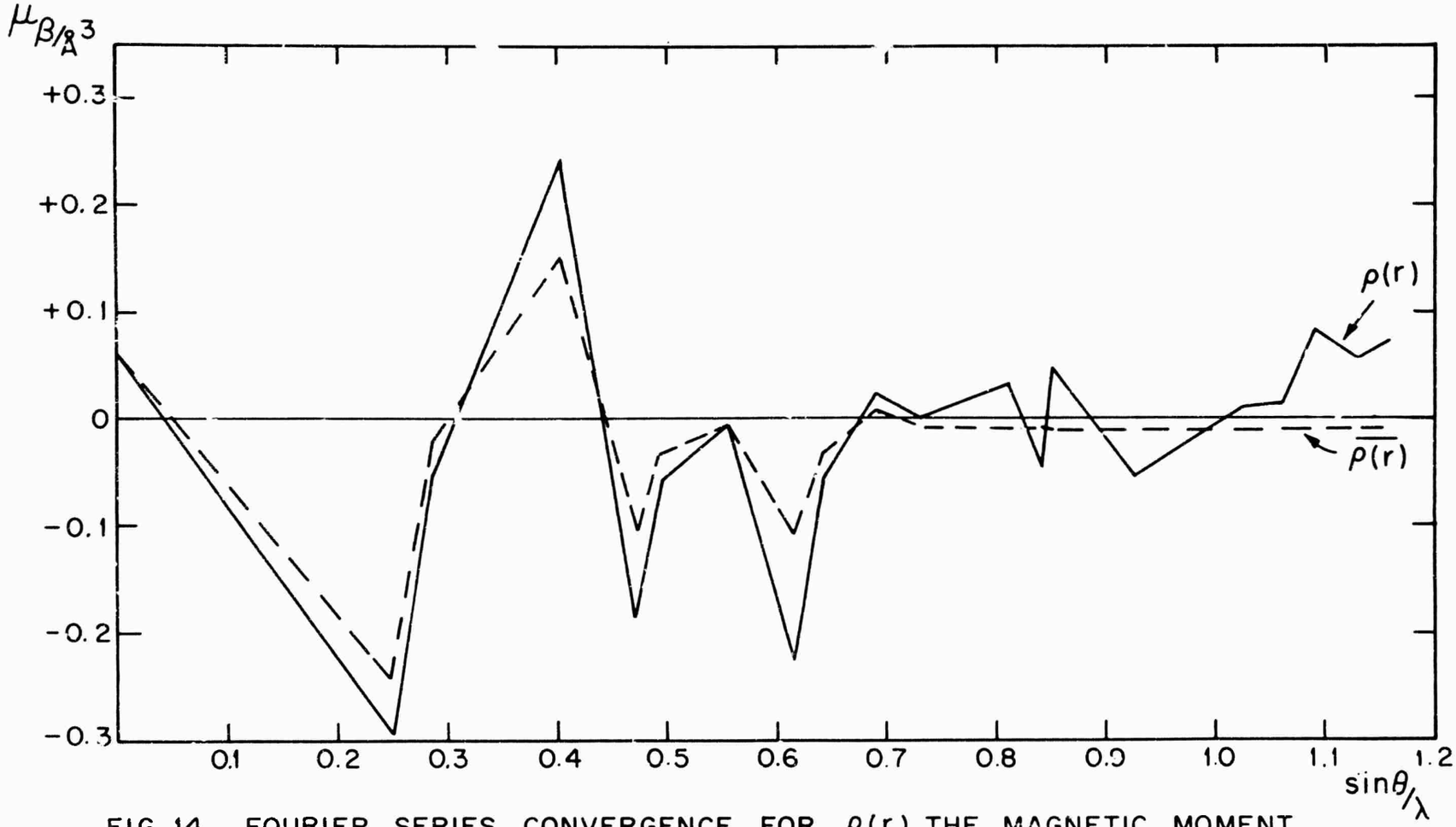

FIG. 14 FOURIER SERIES CONVERGENCE FOR $\rho(r)$ THE MAGNETIC MOMENT DENSITY AND FOR $\overline{\rho(r)}$ THE MAGNETIC MOMENT DENSITY AVERAGED OVER A CUBIC BLOCK 0.15 LATTICE CONSTANTS ON A SIDE.

region near the atoms. $\overline{\rho}$ (r) is plotted in Fig. 15 for the direction along the [100] axis. Note that the moment density hump near the origin is spread out more than in Fig. 13, and the value of the moment density at the atomic site is therefore decreased. The $\overline{\rho(r)}$ in other directions in the crystal is similar to $\overline{\rho(r)}$ along [100], the part of the density in the 3d hump being slightly different in different directions due to the high t_{2g} symmetry.

The magnetic moment density in the [100] and [110] planes is shown on the contour maps, Figs. 16 and 17. These maps again emphasize the strong asymmetry in the magnetic moment distribution. The moment density extends out along the [111] body diagonal direction showing the effect of the t_{2g} symmetry of the 3d magnetic electrons. The part of the moment density near the atomic sites in the 3d magnetic moment humps was given by the series for $\rho(r)$. The series for $\overline{\rho(r)}$ was employed to give the moment density far from the lattice points. The Fourier maps show that the magnetic moment density consists of large positive humps near the atomic sites imposed on a small constant negative background of about 0.0085 $\mu_\beta/\text{A}^{\circ 3}$. This is in very good agreement with the model of the magnetization obtained in Section B. This model required that at 0°K a negative moment density of 0.0096 $\mu_\beta/\text{A}^{\circ 3}$ be spread uniformly over the unit cell. At room temperature, the constant negative contribution would be about 0.0091 $\mu_\beta/\text{A}^{\circ 3}$ which agrees closely with that seen in the moment density maps.

It is worthwhile to emphasize that the Fourier inversion technique requires no theoretical model of the magnetic moment distribution, and gives the spatial distribution of the magnetic moment density directly from the measured data.

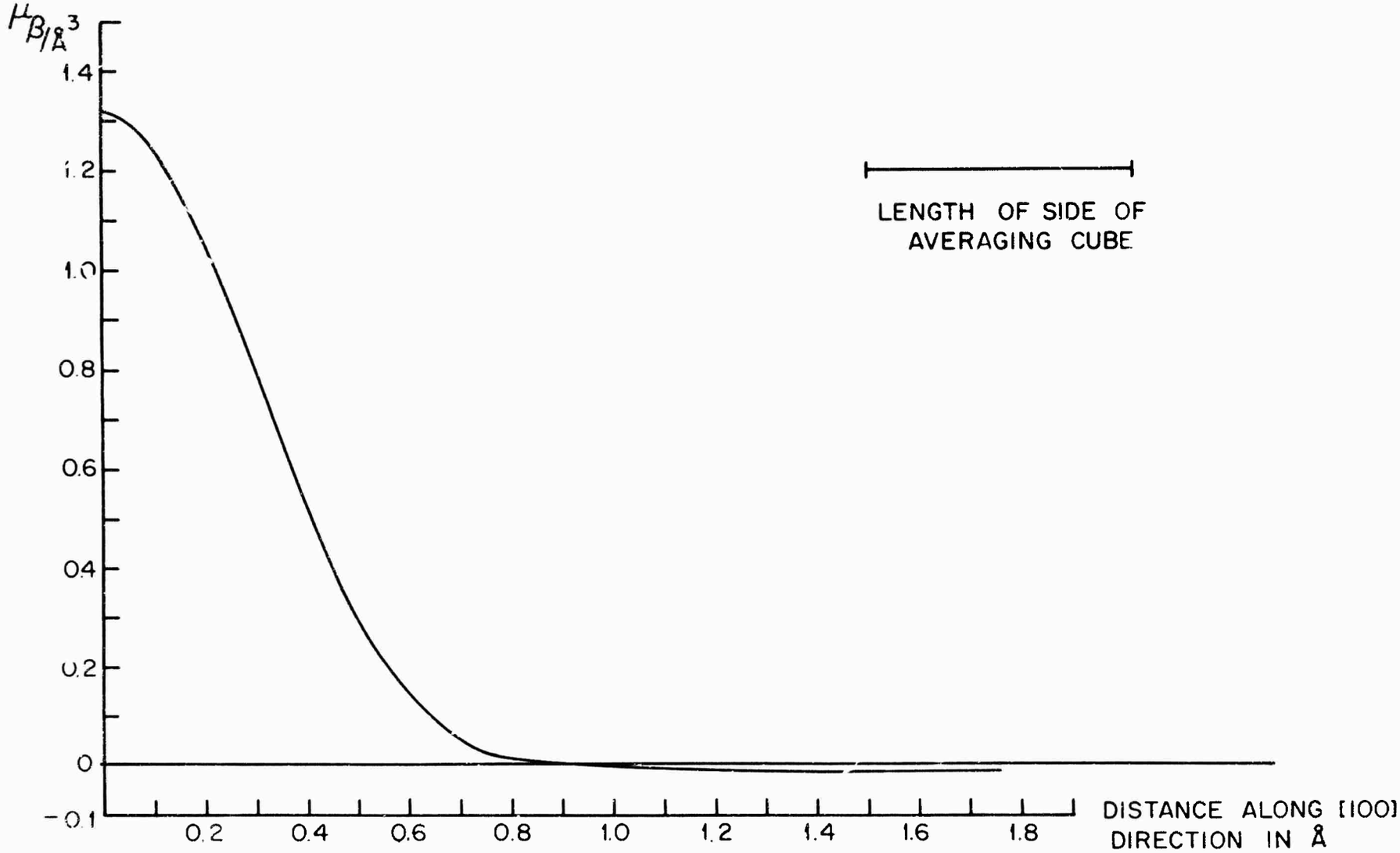

FIG. 15 $\overline{\rho(r)}$ FOR A CUBIC BLOCK 0.15 LATTICE CONSTANTS ON A SIDE PLOTTED ALONG THE [100] DIRECTION

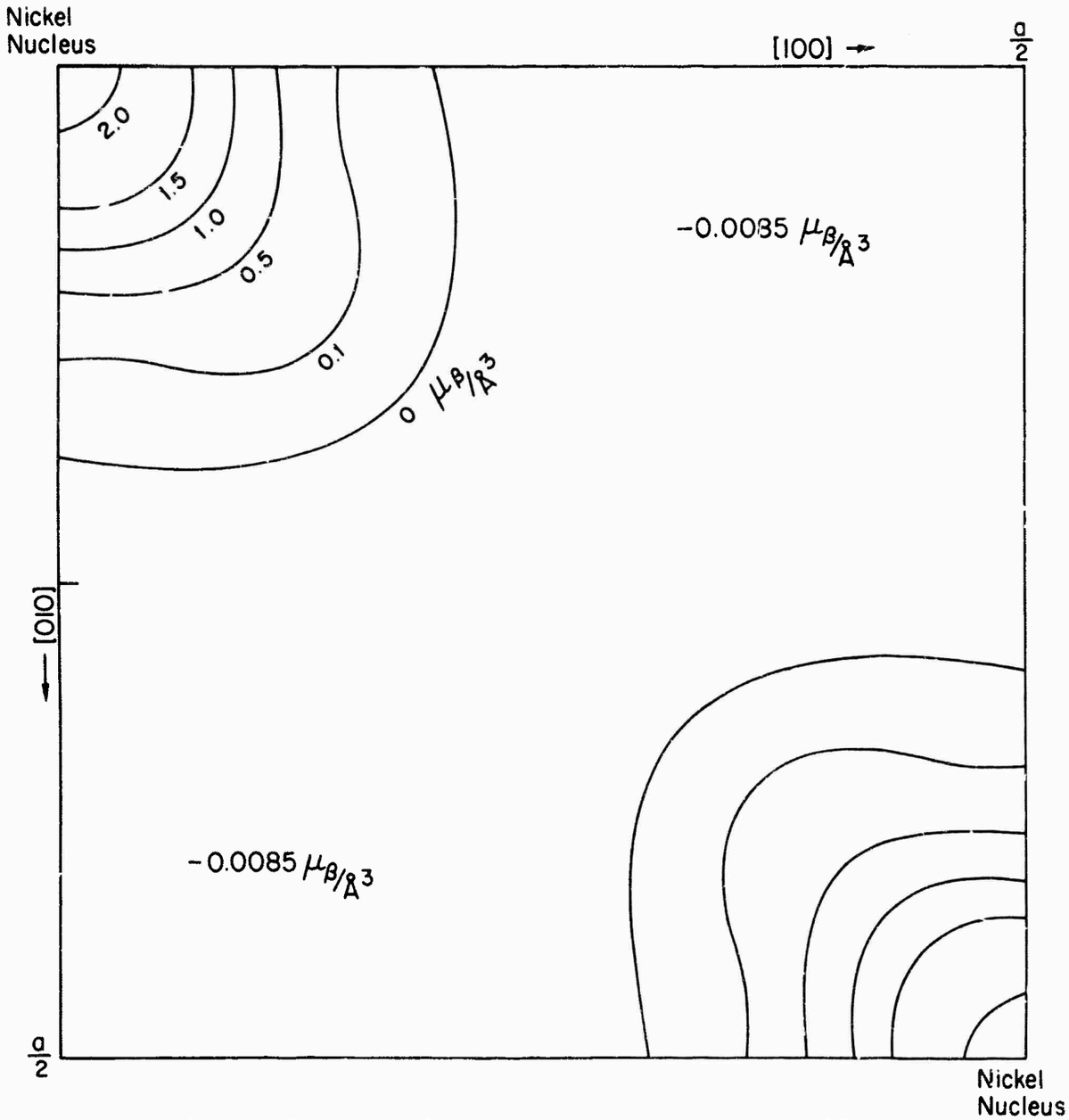

Fig. 16 Magnetic Moment Distribution in the [100] Plane

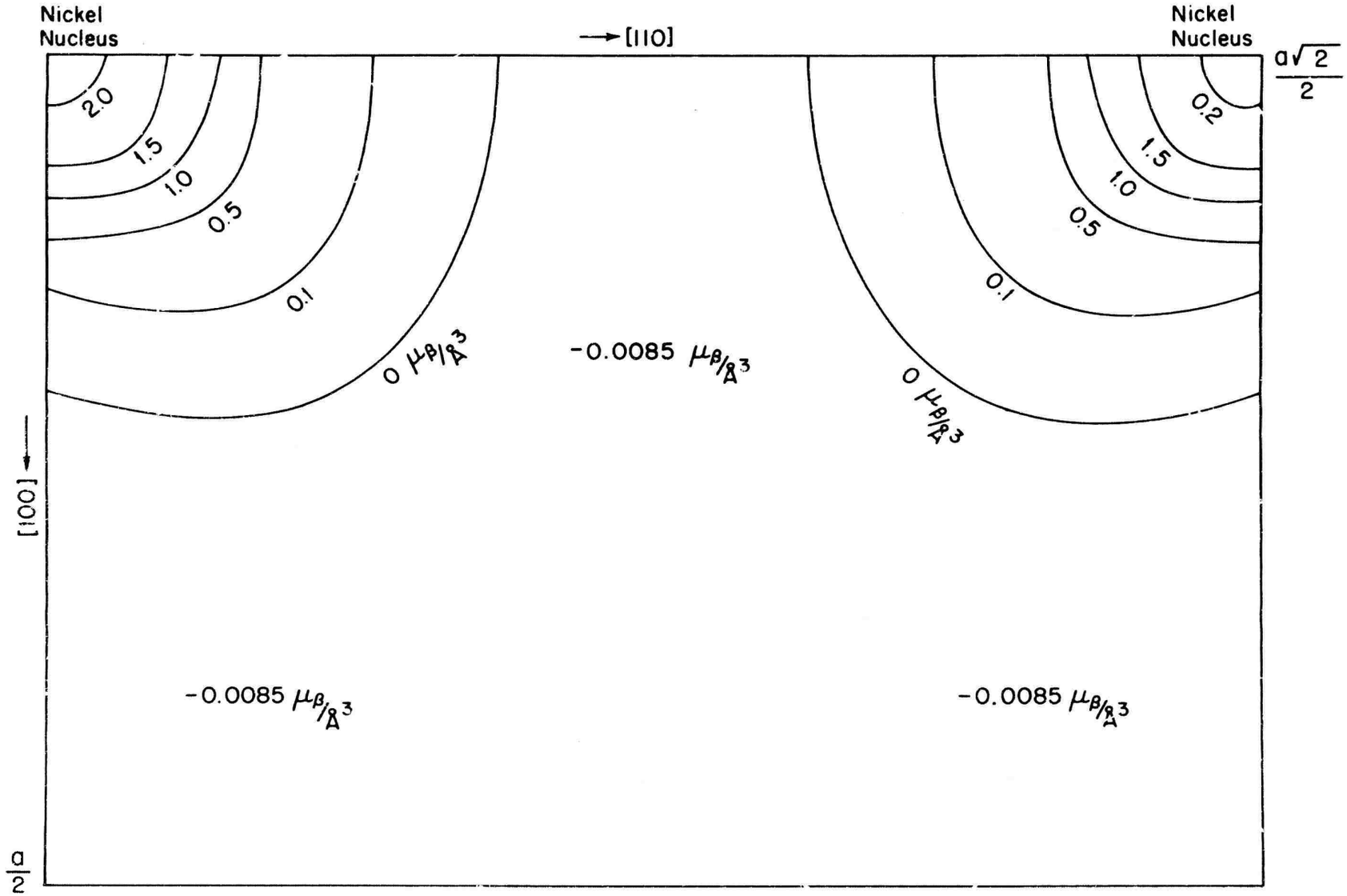

Fig. 17 Magnetic Moment Distribution in the [110] Plane

D. Summary

The magnetic form factor of nickel has been determined for the first 27 reflections, which corresponds to a $\frac{\sin\theta}{\lambda}$ value of 1.16 A^{o-1}. The magnetic form factor contains information about the spatial distribution of the magnetic moment density in the unit cell. There are two approaches one can take in obtaining this information. The first is to compare the measured form factor with calculated form factors. Unfortunately, there are no calculated form factors available for nickel metal, but a number of free atom form factors are available for several stages of ionization. It is surprising to find that the free atom form factor for $Ni^{\#}$ fits the data extremely well, provided a uniform negative contribution is added to the moment density. We are unable to determine the origin of the negative contribution but feel that negatively polarized 4s electrons, or spin polarization effects in the 3d band, could be responsible. The form factor is not a smooth function of $\frac{\sin\theta}{\lambda}$, and from the comparison with the free atom form factor we find that $81\pm1\%$ of the 3d electrons occupy t_{2g} orbitals regardless of the origin of the negative contribution to the magnetization.

The second approach in analyzing the data is to Fourier-transform the form factor to obtain a three-dimensional map of the moment distribution. The Fourier series gives accurate information about the shape of the moment density near the lattice points, but converges too slowly to give any information in the region between the atoms where the moment density is small. A Fourier series was devised that gives the density averaged in space over a cubic block. This series smears out the moment distribution somewhat but converges quickly giving accurate information in the region where the moment density is small. A map of the moment density derived from these Fourier series shows the t_{2g}

symmetry clearly and pictures the moment distribution as being similar to asymmetric free atom distributions placed on a uniform negative background. The two approaches to analyzing the data give very similar results for the size of the negative background and appear to be consistent with each other in every way.

BLANK PAGE

APPENDIX A

INSTRUMENTAL CORRECTIONS

For the half wavelength correction we must know $\frac{I_{\lambda/2}}{I_\lambda}$. Moon [11] measured this ratio for the S-4 spectrometer by determining the integrated intensity for the same reflection from the same crystal for both wavelength components. This measurement had to be corrected for the difference in crystal reflectivity and absorption for the two wavelengths to obtain the incident beam intensity ratio from the reflected intensity ratio. The measurement was checked by inserting a Pu filter in the beam which at 1.05A^{o} removes practically all the $\lambda/2$ component. Previous values obtained in the laboratory for the ratio of $I_{\lambda/2}$ to I_λ were $\frac{I_{\lambda/2}}{I_\lambda} = 0.011$. This number does not have to be known accurately as the $\lambda/2$ correction to the data is very small in all cases.

The polarization is determined by using an analyzing crystal similar to the polarizing crystal and measuring the flipping ratio. The polarization is not uniform over the entire beam and in particular is lower in the upper and lower edges of the beam compared to the middle. The form factor measurements were all made using just the middle section of the beam over which the polarization is quite uniform. With the analyzing crystal in the beam, the flipping ratio is given by

$$R_a = \frac{1 + P_a P_o + \frac{I_{\lambda/2}}{I_\lambda}\frac{g_{\lambda/2}}{g_\lambda}}{1 - P_o P_a (2f-1) + \frac{I_{\lambda/2}}{I_\lambda}\frac{g_{\lambda/2}}{g_\lambda}} \qquad \text{(A-1)}$$

making use of equation (2-9) and letting

$$P_a = \frac{g_a^+ - g_a^-}{g_a^+ + g_a^-} \qquad (A\text{-}2)$$

where g_a^+ and g_a^- are the reflectivities of the analyzing crystal. P_o is the beam polarization at the test crystal position and can be thought of as being the product of P_p, the polarizing efficiency of the polarizer, and P_b which represents the beam depolarization along the path between the polarizing and analyzing crystals. The half wavelength terms require a knowledge of $g_{\lambda/2}/g_\lambda$ which can be calculated using the form factor data for $Co_{.92}Fe_{.08}$ of Nathans and Paoletti [41].

The shim ratio is given by

$$S = 1 + P_o P_a \qquad (A\text{-}3)$$

This ratio S is defined as the ratio of the reflected intensity from a polarized beam to the reflected intensity for the same beam completely depolarized. The beam is depolarized by inserting a steel shim in the beam. Moon found for the S-4 spectrometer $S = 1.997 \pm .004$ and $R_a = 97 \pm 1$. Using (A-1) and (A-3) this gives $(1-2f) = 0.985 \pm 004$. The nickel measurements were taken using a different magnet and for this magnet $R_a = 84 \pm 2$. It is reasonable to assume that this smaller value of R_a was caused by a decrease in P_o rather than in (1-2f) so we can let $(1-2f) = 0.985 \pm .004$ in our case also.

The analyzing crystal is in a larger magnet than the polarizing crystal so it is expected that $P_a \geq P_p$ if the two crystals are cut from the same ingot. Flipping ratios as high as 200 have been measured with the analyzing crystal on the S-3 spectrometer. In this case, even if P_p and (1-2f) are taken to be 1 this give $P_a = 0.995$, so it is a very good assumption to set $P_a = 1$ in our calculations. Using $R_a = 84$ we then obtain $P_o = 0.992$,

which is the value that was used for making the depolarization corrections.

The above values for P_o, (1-2f) and P_a are the most reasonable ones considering the experimental information available. It is found, however, that P_o, (1-2f) and P_a are very restricted if a flipping ratio of 84 is obtained with the analyzing crystal. Within the restriction R_a=84 and $P_a \geq P_p$ any assignment of values for P_o, (1-2f) and P_a give the same polarization correction to the data within the experimental error.

Some of the higher reflections were measured at a wavelength of 0.77 Å. The flipping ratio for the analyzing crystal in this case was 42. The polarization corrections at this wavelength were made using (1-2f) = 0.985, P_a=1, and P_o = 0.968. The data are very insensitive to the assignment of these values since only reflections with R very close to 1 were measured at 0.77 Å.

BLANK PAGE

APPENDIX B

CRYSTALS

The nickal crystals were grown at the neutron diffraction laboratory by the Briugman method. The melt was contained in a pointed alumina crucible and heated by means of a 2 1/2 kW high frequency generator. Once the crucible was correctly aligned the vacuum system containing the crucible was evacuated to a pressure of 10^{-5} mm/Hg and outgassed for several hours. When the outgassing was complete one half of an atmosphere of helium was let into the crucible through a molecular sieve. The molecular sieve served to remove impurities such as oxygen from the helium gas. The crystals were grown over a period of about 12 hours in the helium atmosphere. Various growing rates and temperatures were tried in order to get crystals with a uniform mosaic spread throughout the crystal volume. The nickel used was supplied by the Johnson Matthey and Co. in rod form. The largest impurity present was iron which was present to the order of 5 parts per million. Smaller amounts of other impurities were present but the nickel was sufficiently pure so that no corrections were needed to be made to form factor data due to the presence of impurities.

The crystals were oriented roughly by X-rays and then more precisely by neutrons. The entire experiment was doen with two crystal ingots, one oriented to give sample slices perpendicular to the (110) direction, the other orientated to give (100) slices. The crystal ingots were cut into slices 0.050 inche thick with an alundum wheel. These slices were then polished to the thickness desired by using various abrasive papers and diamond paste. Crystal slices as thin as 0.001 inch and uniform in thickness to 0.0001 inch could be obtained. By means of a series of etchings and X-ray measurements, the crystal slices prepared in this manner were found to have a fairly

uniform mosaic spread throughout their thickness. Crystal slices less than 0.005 inch thick tended to bend slightly after polishing, producing a wide mosaic width. The wide mosaic width in the thin slices was useful in reducing secondary extinction.

APPENDIX C

SAMPLE DEPOLARIZATION

In order to determine the depolarization of a crystal slice tilted in a magnetic field, the direction of the magnetization inside the sample must first be obtained.

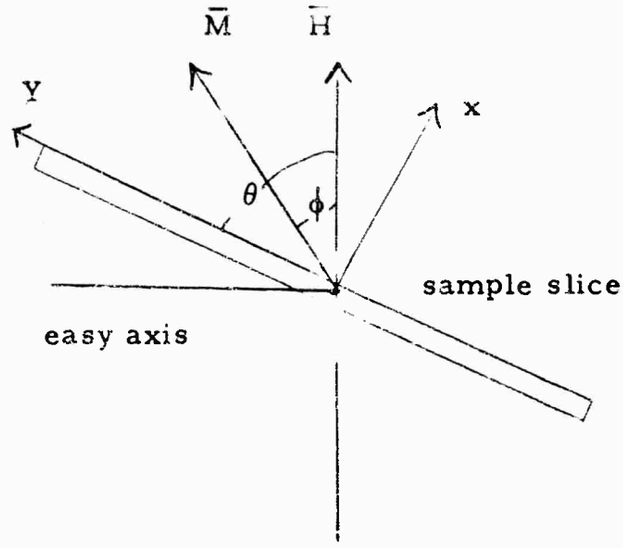

Fig. 18

Coordinate System for Depolarization Calculations

Let $\bar{H}$ be the field outside of the sample and $\bar{H}_i$ be the field inside the sample. Let N_x and N_y be the sample demagnetizing factors. Then

$$\bar{H}_{ix} = \bar{H}_x - 4\pi N_x \bar{M}_x$$

$$\bar{H}_{iy} = \bar{H}_y - 4\pi N_y \bar{M}_y \qquad \text{(C-1)}$$

$$M_x = M \sin(\theta - \phi)$$

$$M_y = M \cos(\theta - \phi) \qquad \text{(C-2)}$$

The total magnetic energy can then be written letting $(\theta - \phi) = \beta$.

$$E_m = C + K_1(\alpha_1^2\alpha_2^2 + \alpha_2^2\alpha_3^2 + \alpha_3^2\alpha_1^2) + K_2(\alpha_1^2\alpha_2^2\alpha_3^2) +$$
$$MH\cos\phi - 4\pi N_x M^2 \sin^2\beta - 4\pi N_y M^2 \cos^2\beta \qquad (C-3)$$

where the αs are the direction cosines between the easy axis and the external field direction. For nickel, $K_1 = -35000 \frac{ergs}{cm^3}$ $K_2 = 40000 \frac{ergs}{cm^3}$ and $M = 485 \frac{ergs}{gauss\ cm^3}$ [42, 32]. The experiment was done in a field strength of H= 7.2 koe. The magnetic field energy terms are almost two orders of magnitude larger than the anisotropy energy terms and it is a very good approximation to neglect anisotropy altogether.

We want to minimize the energy with respect to ϕ so we set $\frac{\partial E}{\partial \phi}$ equal to zero giving

$$\frac{\cos\beta \sin\beta}{\sin\phi} = \frac{H}{8\pi (N_x - N_y)} \qquad (C-4)$$

The demagnetizing factors N_x and N_y are given by Osborne [43] if the sample shape is approximated by an ellipsoid. For any major to minor axis ratio on the order of our sample size $N_x = 1$, $N_y = 0$. Given an angle θ equation (C-4) can be solved graphically for the angle ϕ which gives the direction of $\bar{M}$ inside the sample. The polarization direction is along $\bar{B}$ and once $\bar{M}$ is found $\bar{B}$ is given by equation (2-36).

Now consider the depolarization resulting from neutrons originally polarized in the direction of $\bar{H}$ traversing a sample slice in which the direction of the $\bar{B}$ inside is different than the externally applied $\bar{H}$. Halpern and Holstein [28] show that this problem may be treated classically. The change in spin axis of a neutron passing through a magnetic region is given by the classical equation of motion

$$\frac{d\bar{S}}{dt} = g\,\bar{S} \times \bar{B} \qquad \text{(C-5)}$$

where $\bar{S}$ is the operator for the neutron spin and g is the gyromagnetic ratio of the neutron. This equation is linear in the spin operator so the spin operator can be replaced by its expectation value. If the neutron passes through a region i with field $\bar{B}_i$, equation (C-5) shows that the change in the spin is such that the component parallel to $\bar{B}_i$ is unchanged and the component perpendicular to $\bar{B}_i$ precesses about $\bar{B}_i$ with angular velocity $\bar{\omega}_i = g\,\bar{B}_i$. We can thus write

$$\bar{S}_i = A_i\,\bar{S}_i - 1 \qquad \text{(C-6)}$$

where A_i is the dyadic

$$A_i = \frac{\bar{B}_i\,\bar{B}_i}{B_i^2} + \left(1 + \frac{\bar{B}_i\,\bar{B}_i}{B_i^2}\right)\cos\omega_i t - (\sin\omega_i t)\,\frac{\bar{B}_i x}{B_i}$$

Since the initial polarization is very good, the initial spin may be written $S_o = \hat{k}$ where $\hat{k}$ is a unit vector in the direction of $\bar{H}$. We will choose a coordinate system so that $\hat{j}$ is along the axis of tilt of the sample and x, y, and z are measured along the coordinate axes so defined. Inside the sample which we will call region 1 the spin is given by

$$\bar{S}_1 = \frac{\hat{i}\,B_1^x + \hat{k}\,B_1^z}{B_1}\,[1-\cos\omega_1 t]\cos\gamma + \hat{k}\cos\omega_1 t$$

$$+ \hat{j}\sin\omega_1 t\sin\gamma \qquad \text{(C-7)}$$

where t is the time the spin is observed measured from the time the neutron entered the sample, and γ is the tipping angle of magnetic field in the slice. The polarization at the position where the neutron leaves the slice is given by setting t equal to the neutron transit time T in the slice. The

neutron spin after leaving the slice $\bar{S}_f$ is found by applying (C-6) again giving

$$\bar{S}_f = [(1-\cos\omega_1 T)\cos^2\gamma + \cos\omega_1 T]\hat{k} \qquad \text{(C-8)}$$

where we have averaged over time to get the quantity of interest for the experiment. The final neutron polarization P_T can be obtained directly from (C-8) and the flipping ratio is given by the expression

$$R = \frac{1 + 2p/b\, P_o P_T + (p/b)^2}{1 - 2p/b\, P_o P_f P_T + (p/b)^2} \qquad \text{(C-9)}$$

where P_o is the initial polarization, P_f the flipper polarization and p/b is known for the analyzing crystal. The flipping ratio determined from this expression is compared with an experimentally measured flipping ratio in Fig. 7.

APPENDIX D

THE SUMMARY OF EXPERIMENTAL DATA

A summary of the experimental data is given in Table III. All errors are given in standard deviations. The statistical uncertainty in the measured flipping ratio, R_m, was determined by two methods. The standard deviation was computed from the total number of neutrons counted assuming a normal distribution of counting intensity. This was compared to the standard deviation obtained directly from the data by computing the deviation from the mean for each counting interval. In all cases, the two determinations of the standard deviation agreed very closely. If the standard deviation computed directly from the data is noticeably larger than that determined from the total number of counts, it is an indication that noise or other non-random effects may be entering the electronic counting apparatus and the data should be suspect.

The background counting rate also enters into the statistical error. For very low counting rates the background uncertainty may give a large contribution to the total error. The background was measured on both sides of the Bragg peak in all cases, and for low intensity runs was measured at several positions on each side of the Bragg peak both before and after the flipping ratio measurement was made.

The measured flipping ratio R_m was corrected for instrumental errors using the methods discussed in Chapter II, Section A. The corrected flipping ratio R_{ext} was then converted to p/b and corrected for extinction effects. The error in p/b includes the uncertainties in the size of the corrections applied to the data. Finally, the p/b from the measurements made at each reflection were averaged to obtain p/b avg. A larger number of measurements were

made than are shown in Table III. Some of the measurements had to be discarded because of high extinction or other uncertainties and only the runs that were used to obtain the final average p/b avg are included in Table III.

TABLE III

Summary of Measured and Corrected Experimental Data

hkl	Sin θ/λ	Sample	The Measured Flipping Ratio R_m	The Flipping Ratio Corrected for Extinction $R_{ext.}$	$\Delta P/b$ Extinction	P/b	P /b avg.
(111)	0.246	A-3-1	1.548 ± 0.0013	1.564	0.0072	0.11868± 0.0008	
(111)		A-4	1.563 ± 0.0020	1.578	0.0053	0.11880±0.0009	0.1193±0.0006
(111)		A-2-2	1.600 ± 0.0036	1.618	0.0004	0.12013±0.0007	
(200)	0.284	A-4	1.492 ± 0.001	1.505	0.0041	0.10604±0.0007	0.1058± 0.0006
(200)		B-3-b	1.427 ± 0.001	1.440	0.0147	0.10556±0.0007	
(220)	0.402	A-4	1.292 ± 0.001	1.299	0.0020	0.0672± 0.0005	0.0672±0.0005
(311)	0.472	A-4	1.202 ± 0.002	1.212	0.0006	0.04860±0.0006	0.0483±0.0005
(311)		A-3-2	1.200 ± 0.002	1.205	0.0014	0.04791±0.00066	
(222)	0.493	A-3-1	1.194 ± 0.001	1.198	0.0017	0.04679±0.0004	0.0468±0.0004
(222)		A-4	1.195 ± 0.003	1.200	0.0021	0.04674±0.0008	
(400)	0.569	A-4	1.095 ± 0.001	1.096	0.0006	0.02357±0.0003	0.0236±0.0004
(400)		B-3-b	1.088 ± 0.001	1.096	0.0021	0.02350± 0.0006	
(331)	0.620	A-4	1.102 ± 0.001	1.104	0.0006	0.02533±0.0004	0.0253±0.0004
(420)	0.636	B-3-b	1.073 ± 0.0008	1.075	0.0017	0.0198 ± 0.0004	0.0190±0.0004

hkl	Sin θ/λ	Sample	The Measured Flipping Ratio R_m	The Flipping Ratio Corrected for Extinction $R_{ext.}$	$\Delta P/b$ Extinction	P /b	p /b avg.
(642)	1.063	A-5	1.0003±0.002	1.0003	0.0000	0.0001±0.0005	0.0001±0.0005
(713)	1.091	A-5	0.987 ±0.002	0.986	-0.0001	-0.0040±0.0005	-0.0040±0.0005
(553)	1.091	A-5	1.006 ±0.002	1.006	0.0002	0.0018±0.0005	0.0018±0.0005
(800)	1.137	A-5	0.970 ±0.002	0.968	-0.0014	-0.0091±0.0005	-0.0091±0.0005
(733)	1.164	A-5	0.992±0.002	0.992	-0.0004	-0.0025±0.0005	-0.0025±0.0005

(422)	0.696	A-3-2	1.063 ± 0.002	1.065	0.0005	0.0162±0.0005	0.0162±0.0005
(511)	0.739	A-3-2	1.024 ± 0.003	1.025	0.0002	0.00620±0.0007	0.0054±0.0005
(511)		A-4	1.019 ± 0.002	1.020	0.0001	0.00499±0.00052	
(333)	0.739	A-3-1	1.064 ± 0.002	1.065	0.0007	0.0163±0.0004	0.0165±0.0004
(333)		A-4	1.067 ± 0.003	1.068	0.0005	0.0168±0.0007	
(440)	0.804	A-4	1.033 ± 0.002	1.034	0.0003	0.0087±0.0005	0.0087±0.0005
(531)	0.841	B-3-6	1.016 ± 0.002	1.017	0.0006	0.0048±0.0005	0.0048±0.0005
(600)	0.853	A-4	0.988 ± 0.002	0.988	-0.0002	-0.0032±0.0005	-0.0037±0.0004
(600)		B-3-6	0.986 ± 0.001	0.986	-0.0005	-0.0038±0.0003	
(442)	0.853	A-4	1.030 ± 0.002	1.031	0.0004	0.0079±0.0005	0.0079±0.0005
(620)	0.899	B-3-b	0.995 ± 0.002	0.995	-0.0001	-0.0014±0.0005	-0.0014±0.0005
(533)	0.932	A-5	1.006 ± 0.002	1.006	-0.0002	0.0017±0.0005	0.0017±0.0005
(622)	0.943	A-5	1.003 ± 0.002	1.003	0.0001	0.0008±0.0005	0.0008±0.0005
(444)	0.984	A-2-1	1.020 ± 0.003	1.021	0.0003	0.0054±0.0008	0.0056±0.0005
(444)		A-5	1.020 ± 0.002	1.021	0.0006	0.0056±0.0005	
(551)	1.015	A-5	1.005 ± 0.002	1.005	0.0002	0.0014±0.0005	0.0014±0.0005
(711)	1.015	A-5	0.976 ± 0.002	0.975	-0.0008	-0.0071±0.0005	-0.0071±0.0005
(640)	1.025	A-5	0.9997± 0.002	0.9997	0.0000	-0.0001±0.0005	-0.0001±0.0005

BLANK PAGE

REFERENCES

1. J. S. Schwinger , Phys. Rev. 51, 544 (1937).
2. O. Halpern and M. H. Johnson, Phys. Rev. 55, 898 (1939).
3. S. Odiot and D. Saint James, J. Phys. Chem. Solids 17, 117 (1960).
4. M. Blume, Phys. Rev. 124 , 96 (1961).
5. M. Blume, Phys. Rev. 130, 1670 (1963).
6. M. Blume, Phys. Rev. Letters 10, 489 (1963).
7. W. Marshall, (unpublished notes).
8. R. Bozorth, Ferromagnetism, D. Van Nostrand Company, Inc., New York, P. 876 (1951).
9. R. Nathans, C. G. Shull, G. Shirane, and A. Andresen, J. Phys. Chem. Solids 10 , 138, (1959).
10. C. G. Shull and Y. Yamada, "Proc. International Conference on Magnetism and Crystallography," Kyoto, 1961 (J. Phys. Soc. Japan, Vol. 17) Supplement B-III, P. 1 (1962) C. G. Shull, Electronic Structure and Alloy Chemistry o. the Transition Elements, Interscience Publishers, New York, P. 69 (1963).
11. R. Moon, "Magnetic Scattering of Neutrons by Hexagonal Cobalt, " Technical Report No. 312, Lincoln Laboratory, Massachusetts Institute of Technology, Cambridge, Massachusetts (1963).
12. S. J. Pickart and R. Nathans, Phys. Rev. 123, 1163 (1961).
13. W. Phillips, Thesis, "A Neutron Diffraction Study of a Palladium - Rich FePd Ferromagnetic Alloy, " Massachusetts Institute of Technology, Cambridge, Massachusetts, (1964).
14. G Shirane, R. Nathans and C. W. Chen, Phys. Rev. 134 , A1547, (1964).
15. C. Herring, J. Appl. Phys. 31,3S (1960.)

16. H. Brooks, Electronic Structure and Alloy Chemistry of the Transition Elements, Interscience Publishers, New York, P. 3 (1963).

17. J. H. Wood, Phys. Rev. 117 , 714 (1960).

18. F. Stern, Phys. Rev. 116, 1399 (1959).

19. R. Nathans, "Proc. International Conference on Magnetism and Crystallography," Kyoto, 1961 (J. Phys. Soc. Japan, Vol. 17, Supplement B-3), P. 7 (1962).

20. R. E. Watson and A. J. Freeman, Phys. Rev. 120, 1125 (1960).

21. G. E. Bacon, Neutron Diffraction, Oxford University Press, London, P. 28 (1955).

22. C. G. Darwin, Phil. Mag. 43, 800 (1922).

23. G. E. Bacon and R. D. Lowde, Acta Cryst. 1, 303, (1948).

24. R. W. James, The Optical Principles of the Diffraction of X-rays, G. Bell and Sons, Ltd, London, P. 221 (1954).

25. W. H. Zachariasen, Theory of X-ray Diffraction in Crystals, John Wiley and Sons, Inc., New York, P. 123 (1951).

26. H. Ekstein, Phys. Rev. 83, 721 (1951).

27. R. M. Moon and C. G. Shull, Acta Cryst. 17, 805 (1964).

28. O. Halpern and T. Holstein, Phys. Rev. 59, 960 (1941).

29. P. Weiss, quoted in R. Bozorth, Ferromagnetism, D. Van Nostrand Company, Inc., New York, P. 270 (1951).

30. F. Menzinger and A. Paoletti, Phys. Rev. Letters 10, 290 (1963).

31. A. W. Saenz, Phys. Rev. 119, 1542 (1960).

32. C. Kittel, Introduction to Solid State Physics, 2nd. ed., John Wiley and Sons, Inc., New York, P. 407 (1962).

33. G. G. Scott, "Proc. International Conference on Magnetism and Crystallography," Kyoto, 1961 (J. Phys. Soc. Japan, Vol. 17, Supplement B-1) P. 372 (1962).

34. R. J. Weiss and A. J. Freeman, J. Phys. Chem. Solids 10, 147 (1959).

35. R. E. Watson and A. J. Freeman, Acta Cryst. 14, 27, 231 (1961).

36. R. E. Watson and A. J. Freeman, Phys. Rev. 120, 1134 (1960).

37. A. J. Freeman, (private communication).

38. L. Hodges, N. D. Lang, and H. Ehrenreich, (private communication).

39. R. J. Weiss, (private communication).

40. W. Sly and D. Shoemaker, MIFRI Two-and-Three Dimensional Crystallographic Fourier Summation Program.

41. R. Nathans and A. Paoletti, Phys. Rev. Letters 2, 254 (1959).

42. K. Honda, H. Masomoto, and Y Shirakawa, quoted in Bozarth Ferromagnetism, D. Van Nostrand Company, Inc., New York, 569 (1951).

43. J. A. Osborne, Phys. Rev. 67, 351 (1945).